scientific reports

Check for updates

OPEN

3D upper crustal structure modelling in southwestern Sicily through multiapproach onshore–offshore data: insight into Sciacca Geothermal Field

Giuseppe Francesco Rizzo[1,2]✉, Mariagiada Maiorana[1], Maurizio Gasparo Morticelli[1,3], Valeria Lo Presti[1], Mauro Agate[1,3] & Attilio Sulli[1,3]

This study investigates the architecture and structural setting of the Sciacca Fault System (SFS), a key component of the Sciacca Geothermal Field in southwestern Sicily, through an integrated geological and geophysical approach. The analysis correlates the offshore SFS lineament with the onshore Mt. Kronio fault system to assess their role in regional deformation and geothermal connectivity. Seismic reflection data reveal a NE–SW oriented transpressive fault network characterized by thrusts and positive structures, with evidence of recent compressive deformation affecting both Upper Calabrian deposits onshore and Late Pleistocene–Holocene sequences offshore. High-resolution profiles show active fluid migration, suggesting a hydraulically connected onshore–offshore geothermal system. A 3D reconstruction of the fault network defines the geometry and extent of the geothermal reservoir and supports a fluid migration model involving a northward and upward flow from a deep source in the offshore sector. Fluids are channelized within fault-bounded compartments sealed by low-permeability surfaces and capped by pelagic units, forming a partial structural trap. Vertical migration culminates where the carbonate substrate is exposed, as at Mt. Kronio, while offshore fluid ascent follows permeable faults and discontinuities within the sedimentary cover.

Keywords 3D geological modelling, Sciacca Fault System, Southwestern Sicily, Sciacca Geothermal System, Geothermal reservoir

In recent decades, the integration of onshore geological data and marine geophysical data has played a key role in studying onshore-offshore transitions, especially in tectonically active regions[1], and references therein). In particular, understanding the three-dimensional architecture of geological structures extending from the continent to the marine sector is fundamental for reconstructing the tectonic evolution of complex areas and assessing associated geological hazards[2–7] or their geothermal potential[1,8]. Most geothermal resources are associated with plate-margin settings, where crustal deformation, magmatism, and fault-controlled fluid flow interact dynamically (The Geysers, California; The Svartsengi, Iceland)[9,10]. Comparable integrated studies in plate-margin geothermal systems have demonstrated that correlating onshore and offshore fault systems is essential for constraining fluid pathways and heat flow distribution[11,12]. Building on insights from global plate-margin geothermal systems, the southwestern Sicily region provides an ideal natural laboratory to study the coupling between onshore–offshore structures and deep fluid flow.

In the study area (Fig. 1) the compressive and transpressive structures characterizing the Sicilian-Maghrebide belt show potential continuity between the emerged and submerged domains, but their structural correlation often remains poorly defined.

Currently, while structures in Sciacca offshore area (Fig. 1) are well documented through seismic profiles and well data (Fig. 2)[1,14,21–24], the connection with onshore outcropping structures, particularly in the Mt. Kronio sector, has not yet been thoroughly verified. This correlation gap compromises the ability to depict a coherent geometry and to correctly reconstruct the deformation kinematics. Furthermore, although extensive

[1]Department of Earth and Marine Science, University of Palermo, Palermo, Italy. [2]Department of Earth Science and Geo-Environment, University of Bari, Bari, Italy. [3] Istituto Nazionale di Geofisica e Vulcanologia, Osservatorio Nazionale Terremoti, Rome, Italy. ✉email: giuseppefrancesco.rizzo@unipa.it

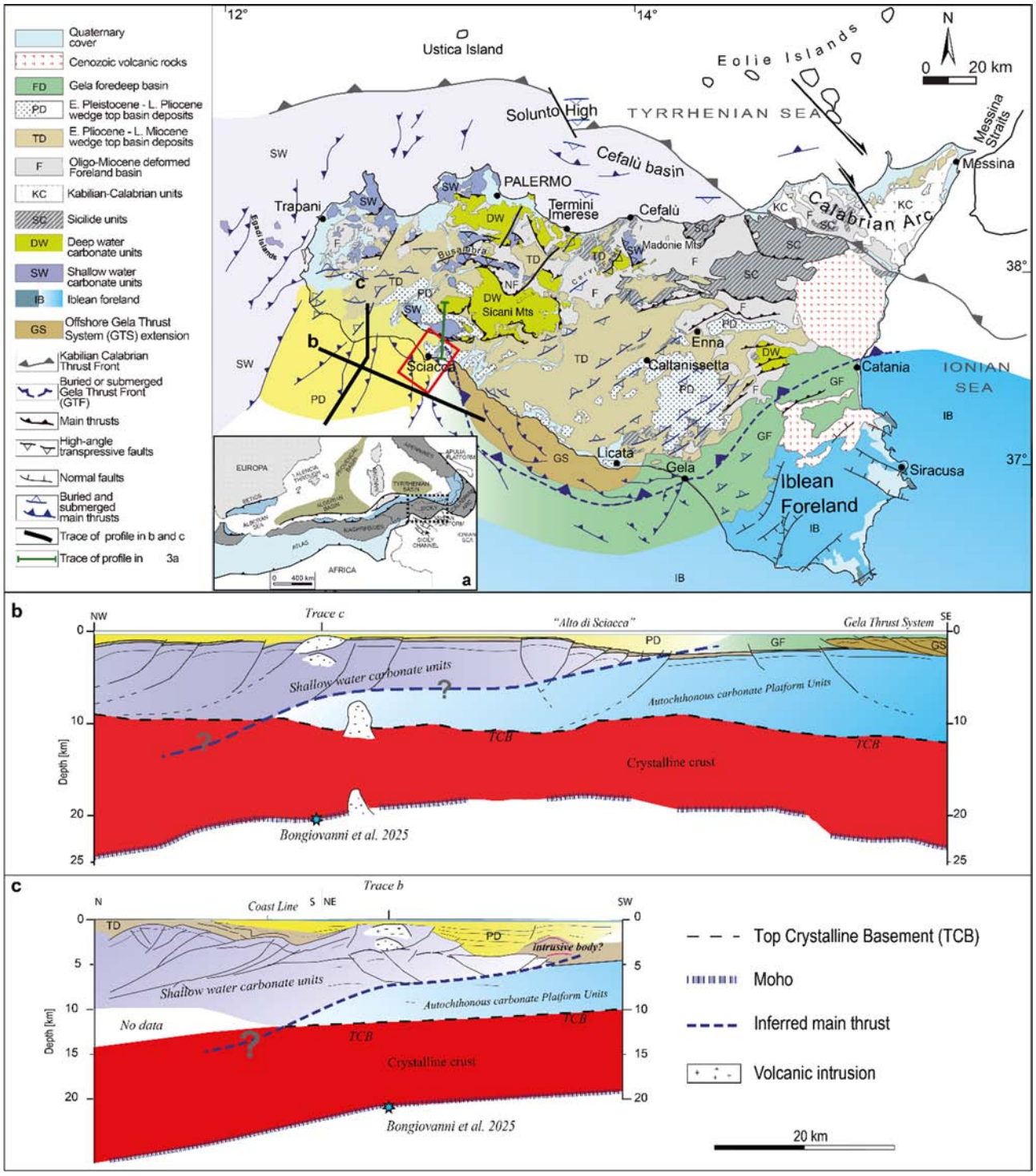

Fig. 1. Structural map of Sicily (from[13–15]), The inset maps show: (**a**) Schematic tectonic map of central-western mediterranean area; (**b**) Interpreted structural-stratigraphic cross-section of the central sector of the CROP M23 seismic profile (from[14,16–19]) across the offshore of Sciacca; (**c**) Central segment of the crustal section across the central Mediterranean, from the Drepano Front to Pantelleria. The section illustrates a reconstruction of the deep structural framework of western Sicily (from[18,20]). Maps and cross-section were generated using Inkscape Software version 1.4 (https://inkscape.org/release/inkscape-1.4.2/windows/64-bit/msi/dl/).

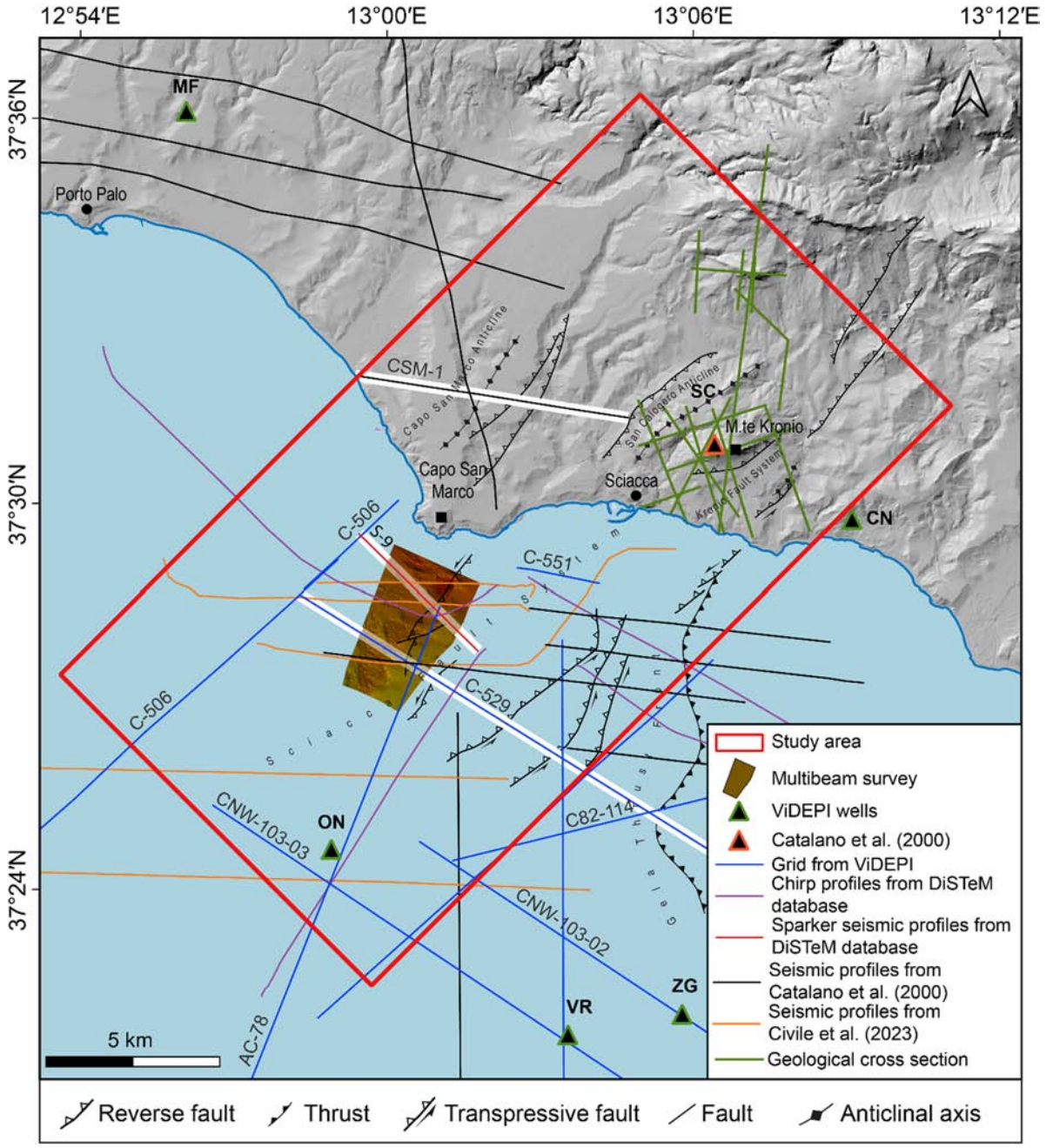

Fig. 2. Trace of seismic lines and geological cross sections analyzed in this work. The white buffer highlights profiles shown in the pertinent Figures (C-529 and CSM-1 in Fig. 6; S-9 in Fig. 7). The plotted wells are: Menfi-1 (MF); Sciacca-1 (SC); Cianciana-1 (CN); Orione-1 (ON); Zagara-1 (ZG) Venere-1 (VR). The tectonic feature derived from[19]. Maps generated using QGis software version 3.34.11 (https://download.qgis.org/downloads/) and Inkscape Software version 1.4 (https://inkscape.org/release/inkscape-1.4.2/windows/64-bit/msi/dl/). Dem used in the maps is from TINITALY (https://tinitaly.pi.ingv.it/).

deep fluid circulation systems are known offshore[1,25–27], their relationship with tectonic structures and onshore surface manifestations[28–31] remains unclear. To understand the active deformation processes and fluid–structure dynamics within the Sicilian orogenic system, it is necessary to systematically integrate onshore and offshore data.

Geological manifestations of endogenous origin are directly linked to active subsurface processes, with their source located vertically beneath the surface expression (i.e. Larderello, volcanic systems, Campi Flegrei)[32–34]. However, this is not always the case: the source of geological processes may be spatially displaced relative to the area of surface occurrence, with subsurface structural configurations controlling fluid circulation. Within this framework, reconstructing a detailed subsurface geological model becomes essential.

The region has long been a focus of exploration activity, as evidenced by numerous research permits, extensive seismic surveys, and several exploratory wells reported in the public ViDEPI database (https://www.videpi.com/videpi/videpi.asp), all highlighting the hydrocarbon potential of the Sciacca offshore and adjacent areas of the Sicilian Channel.

The coexistence of thermal anomalies, deep-seated faults, and fluid circulation patterns in this area suggests a complex interplay between tectonic, geothermal, and hydrocarbon systems along the continental margin.

To address these issues, we carried out a multidisciplinary analysis in the Mt. Kronio—Alto di Sciacca area, aiming to (1) verify the structural continuity between onshore and offshore domains, (2) define the architecture of the potential geothermal reservoir, (3) characterize the kinematics and its implications for crustal deformation, and (4) analyse the distribution and origin of deep fluids, relating them to active tectonic structures and surface evidence. We integrated field data, high-penetration and high-resolution seismic profiles, to build a 3D coherent geological and structural model across the coastal margin.

Geological setting

The geological evolution of the Sciacca region, located in southwestern Sicily and its adjacent offshore, has been shaped by the complex tectonic evolution resulting from the convergence between the African and European plates. This NNW–SSE-oriented convergence, active since the latest Oligocene-Early Miocene[35–38], led to the closure of the Neo-Tethyan Ocean and initiated the progressive collision of the African continental margin with the European domain. This tectonic scenario drove the formation of the Sicilian Fold and Thrust Belt (SFTB), a key segment of the Central Mediterranean orogenic system (Fig. 1b,c)[14,17,18,39–44].

The SFTB is composed predominantly of Mesozoic to Cenozoic carbonate platform and basinal successions originally deposited along the African continental margin, later incorporated into a > 10 km thick pile of NE–SW trending, SE-verging imbricate thrust sheets[18,19,45]. Compressional tectonics shaped the structural architecture of this belt from the Early Miocene to the Early (Middle?) Pleistocene, after which transpressional structures became dominant[15,46–48].

In the study area, the STFB consists of a Meso-Cenozoic carbonate platform succession overlain by Neogene-Quaternary syn-tectonic deposits. In detail, the sedimentary record of the area extends from the Upper Triassic to the Quaternary and is well documented through both onshore outcrops and offshore borehole data[19] and references therein. The oldest unit, the Sciacca Formation (Upper Triassic), is identified in well logs and marks the base of the sedimentary succession,it consists of shallow-water carbonate rocks. The overlying Early Jurassic carbonates record the development of a shallow-water carbonate platform, followed by drowning during the Early-Middle Jurassic, as evidenced by the transition to red nodular limestones. This evolution was succeeded by the deposition of Upper Jurassic to Eocene pelagic limestones with marl and clay intercalations, recording a prolonged phase of hemipelagic sedimentation. An angular unconformity marks the base of the overlying upper Oligocene calcarenites and glauconitic sandstones, indicating a shift to a more proximal marine setting. The Langhian-Tortonian interval is represented by siliciclastic deposits consisting of slightly sandy marls assigned to the San Cipirello Marls unit, which exhibits substantial lateral thickness variations. The lower Pliocene is marked by the Lower Pliocene (Zanclean) age Trubi unit, composed of marly limestones and pelagic marls, and is overlain by Piacenzian–Pleistocene clay-rich units.

A significant Late Pleistocene tectonic phase activated NE–SW and NNE–SSW oriented transpressional fault systems, characterized by left-lateral kinematics and commonly interpreted as a manifestation of ongoing regional deformation. Among these, the Sciacca Fault System (SFS), a prominent NNE–SSW trending fault array, represents a key neotectonic feature that deforms both the offshore domain and the adjacent mainland[19,24,49,50]. These fault systems form a regional lithospheric "transfer zone" affecting the crust and upper mantle to a depth of at least 70 km[51].

A recent tectonostratigraphic reconstruction proposed by Sulli et al.[19] identifies three distinct deformational phases affecting the Sciacca region. The first phase is recorded by contractional structures and angular unconformities within the Oligo-Miocene succession, suggesting regional uplift and subaerial exposure, which in turn inhibited evaporite deposition during the Messinian salinity crisis. The second major compressional phase, occurring during the Upper Pliocene–Pleistocene, linked to the forelandward migration of the orogenic wedge, led to the formation of subparallel thrusts defining the present-day structure of Mt. Kronio[14]. A third, younger extensional phase, overprints the earlier compressional fabric and affects the Pleistocene calcarenites and sands, with NNW–SSE trending faults interpreted as local reactivations of earlier compressional structures[52].

Early structural interpretations of the Mt. Kronio[53–57] highlighted the occurrence of SE-verging thrust systems affecting the Mt. Kronio units, interpreted as part of a broader imbricate thrust wedge.

Offshore, extensive seismic reflection data and deep exploration wells have enabled detailed reconstruction of both the stratigraphy and the structural architecture. The offshore area is characterized by a composite structure involving a deformed foreland overlain by an active fold-and-thrust system, the Gela Nappe, which represents an accretionary prism active since the Late Pliocene until at least 0.8 Ma[58] that emplaced over foreland deposits[21,23–26].

To the west of the Gela Nappe front lies the Alto di Sciacca, a N–S oriented structural high composed of Mesozoic carbonates. This tectonic feature has been variably interpreted as a transpressive belt[21], a strike-slip system[22], or as the frontal part of Thrust System, a wedge over 3 km thick active since the Late Pliocene[23]. The interpretation of the CROP-M23-seismic profile[14] reveals that the external part of the Gela Nappe overlies a relatively shallow crystalline basement, with the crust–mantle boundary (Moho) located at about 9 s two-way travel time (TWT) beneath the Banco Avventura, and rising to 8.5 s TWT offshore of Sciacca (Fig. 1b). The crystalline basement itself lies at depths of approximately 10–15 km (5.5–6 s TWT)[16] (Fig. 1b), indicating a markedly thinned continental crust beneath this sector of the Sicily Channel.

The meso-cenozoic carbonate substrate underlying this sector of the chain has been described as affected by significant extensional fault systems that delineate a possible paleomargin with a NW–SE trend[59]. However, the structural configuration observed by other authors suggests that these pre-existing features may have played a more complex role during the subsequent phases of compressive and transpressive deformation linked to the construction of the Sicilian fold and thrust belt[44,60].

Geothermal background

Sciacca Geothermal Field (SGF) is characterized by hot springs and vaporous manifestations that have been known for millennia and its thermal water has been used for curative purposes[61–63]. Regionally, the SGF is situated along a N-S corridor across western Sicily, where other geothermal fields are present to the North such as Montevago and Alcamo-Castellammare. He-isotope compositions dissolved in samples of SGF waters indicate mantle-derived fluid contribution into the thermal aquifer[29,30]. High thermal gradients, associated with active volcanic areas in the Sicily Channel, indicate that mantle dynamics are closely linked to deep-reaching fault systems[64]. This lithospheric thermal framework provides additional evidence supporting the mantle origin of the fluids feeding the Sciacca Geothermal Field (SGF) and the role of deep crustal discontinuities in channeling heat and magma toward the geothermal reservoir.

The existence of a crustal weakness zone is consistent with historical deep earthquakes which epicenter occurred within the same zone (i.e. Belice Valley earthquake;[29,59]). Magma intrusion into the continental crusts through lithospheric faults, and related upward fluid migration, could provide heat to the overlying sedimentary cover including the SGF. Submarine volcanoes have been mapped and described offshore of SGF, forming a field of volcanic cones and seamounts that extends along the Sicily Channel[65]. Activity ranges from the late Miocene to the Quaternary[66–68]. The morphology, orientation and distribution of these submarine volcanoes suggest a strong structural control by regional fault systems, with magmatism closely linked to extension and later reactivation during compressional tectonic phases in the Sicily Channel[1,68].

In addition, in such offshore area, roughly N-S deep strike-slip faults run from the volcanic banks (e.g. Graham and Terrible banks) to the onshore orogen and they inferred to provide fluid and heat pathways to the offshore continuation of the SGF[1].

Deep faults along such a crustal discontinuity are inferred to have allowed uprising of magma along with mantle-derived fluid which signature is recorded in the geochemical composition of the thermal waters[29]. Heat flow around the Sciacca area is approx. 60 mW/m^2. The caves within the karst system of Mt. Kronio are characterized by warm air flows maintaining a constant temperature of about 37 °C. Water composition data of the SGF are available from several springs and wells. Water from hot springs (e.g. Selinuntine thermal springs, Fig. 3) and wells that tapped into the main Mesozoic aquifer shows temperature of about 55–60 °C[28,29,69]. Top of the thermal water table is approx. at 43 m above sea level[69]. The deepest well drilled in the deep thermal aquifer (Sciacca well, south-east of Mt. Kronio, Fig. 2) reached a depth of approx. 2600 m (below sea level) in the Upper Triassic shallow-water carbonate of the Sciacca Fm. with a bottom temperature of approx. 76 °C[69]. Temperature of the aquifer at 3000 m b.s.l. are estimated in the range of 90–120 °C[70,71].

Overall, the available temperature data from wells and springs show a wide range of values with depth, reflecting significant variability in the thermal conditions of the system.

According to gravimetric data provided by ENI[19], the Bouguer anomaly map displays values ranging from − 47 to 66 mGal (Fig. 11a). This dataset enables the identification and correlation of major structural alignments, both exposed and buried, particularly across the coastal transition zone where other geophysical information is sparse or unevenly distributed. A prominent positive anomaly (50–66 mGal, Fig. 11a) is observed in the western sector, trending NE–SW, and correlates onshore with the relief of Mt. Kronio. This anomaly highlights a physical continuity, albeit disrupted by tectonic discontinuities with the offshore carbonate structural high known as the "Alto di Sciacca"[14], as inferred from seismic reflection profiles and well data.

Fluid pathway

Fluid circulation in structurally complex carbonate systems is widely recognized as being strongly controlled by fault architecture, fracture networks, and their temporal reactivation history. Previous studies have shown that fault zones may act either as conduits or barriers to fluid flow, depending on the internal organization of fault cores and damage zones, as well as on the degree of cementation and cataclasis developed during deformation[73–76] and also for the current filed stress[77]. In carbonate settings, meteoric fluids typically infiltrate through fractured and karstified domains, while deep hydrothermal fluids migrate upward along major fault zones under the simultaneous influence of tectonic stress[78,79]. In the SGF, hydrogeological and geochemical investigations document a vertically organized circulation system involving both shallow meteoric waters and deep hydrothermal fluids hosted in Mesozoic carbonate reservoirs[69,80]. Waters discharged from the main Mesozoic and Paleogene aquifers are characterized by variable $Cl–SO_4$ and Na-Cl compositions. Isotopic relationships (δD vs.Cl^- and $\delta^{18}O$ vs Cl^-) indicate that thermal waters from the deep reservoir result from an approximately 50:50 mixture of meteoric water and modified seawater, while shallower waters show a stronger meteoric signature, a pattern corroborated by Na-Cl ratios[28]). Both shallow and deep waters are enriched in CO_2 and N_2, and helium isotopic compositions measured in the Selinuntine thermal springs reveal a significant mantle-derived gas contribution, pointing to deep fluid inputs ascending along crustal-scale structures[29,30]. Meteoric recharge occurs both locally, through infiltration at Mt. Kronio (Fig. 3), and regionally via Mesozoic carbonate outcrops north of Sciacca (Fig. 3a), whereas deep circulation follows major structural pathways in the crust[72].

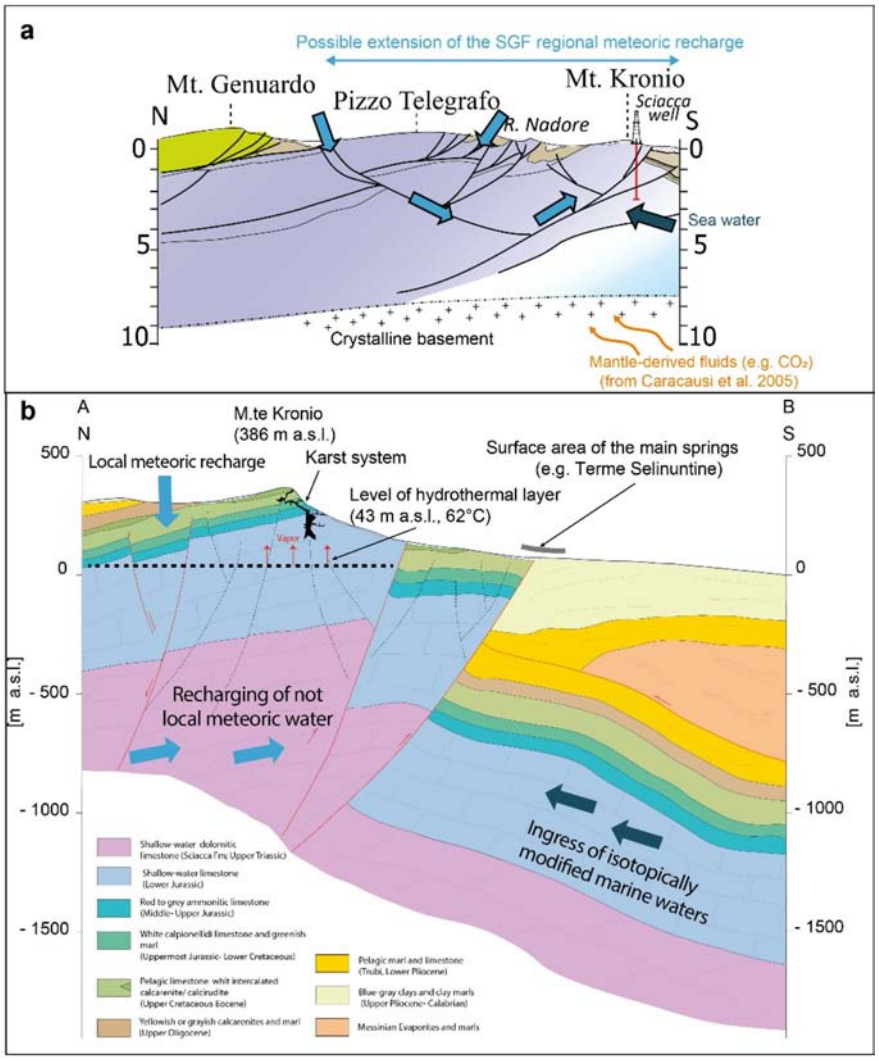

Fig. 3. (**a**) N-S regional cross section showing main elements of the Sciacca Geothermal Field and the possible fluid circulation (from[14,19,72]). For the section trace and legend see Fig. 1; (**b**) N-S geological cross-section across Mt. Kronio showing main hydrological elements. Section trace is located in Fig. 4. Images realized with Inkscape Software version 1.4 (https://inkscape.org/release/inkscape-1.4.2/windows/64-bit/msi/dl/).

Reservoir properties

Carbonate geothermal reservoirs are generally characterized by low primary porosity and permeability, with fluid storage and circulation mainly controlled by secondary porosity generated by fracturing, faulting, and localized dissolution processes[81,82]. Comparable carbonate reservoirs have been described in the offshore Sicily Channel, including the Perla and Vega fields. These reservoirs are composed of partially dolomitized and fractured shallow-water limestones, such as oolitic limestones and algal pelsparites from open-shelf environments (Siracusa and Inici formations)[83]. Porosity in these units is both primary, including intergranular and biomoldic types, and secondary, mainly vuggy, with average values ranging from 12 to 16%. Such lithological and diagenetic characteristics provide effective storage capacity and potential permeability pathways, particularly where enhanced by fracturing and karstification.

Methods

In the study area has been developed of a three-dimensional geological subsurface model, aimed at delivering high-impact, application-oriented geological information. The 3D geological model was constructed in the depth domain by integrating available surface and subsurface data.

Field survey

Surface stratigraphic and structural data were collected during field surveys carried out for Sheet 628 (Sciacca) of the Geological Map of Italy (CARG project).

The deformational patterns associated with faulting were reconstructed through several structural measurement stations located on Mt. Kronio. The mesostructural analysis of fault planes was used to determine

fault orientation, kinematics, and the stress-field directions. Structural data were synthesized using statistical methods, through stereographic projections obtained with Daisy3 software (version 5.38;[84]).

Seismic and well data

A set of geophysical data was used (Fig. 2), including multichannel seismic profiles forming part of the national C-zone profile grid as well as profiles acquired in the framework of oil exploration activities. The former were recorded using an Aquapulse source, with a sampling interval of 2 ms, a recording window of 5 s, 1200% fold coverage. The latter were acquired using an Airgun source with the same sampling interval. For the onshore profiles, the seismic source consisted of dynamite, with a sampling interval of 2 ms.

Seismic profiles were calibrated using wells provided by the ViDEPI public database (source https://www.videpi.com/videpi/videpi.asp): Orione, Venere, and Zagara wells. Positioned close to the seismic lines, these wells allowed for effective calibration of the profiles. To perform a more detailed analysis of the Quaternary portion of the submerged succession, a single-channel seismic reflection survey was carried out in June 2024. During this campaign, seismic sections were acquired using a Geo-Spark 100 source and the Qinsy acquisition software (QPS). The acquired data underwent processing with the Geo-suite AllWorks software, following a workflow that included the following steps: Debias, Infinite Impulse Response (IIR) filtering, Mixing, Muting, Trace Equalization, and Swell Filtering.

Interpretation was carried out using dedicated software for seismic-stratigraphic analysis, identification of tectonic structures, and generation of maps depicting the geometry of key stratigraphic horizons. The dataset was interpreted through seismic-stratigraphic and structural analysis following evaluation of seismic patterns, such as reflector amplitude and frequency, continuity, lateral terminations, configuration and the external shape of reflector packages, as illustrated by[85] to recognize seismic facies unit. This workflow led to the development of a 2.5D geological model using Move (Midland[86]) software.

Model reconstruction

The three-dimensional model reaches a maximum depth of −6000 m below sea level and provides a good-resolution representation of the geometry of the main geological bodies and structural discontinuities. The 3D model covers an area of approximately 22 × 18 km and was built with a grid resolution of 200 m in both the horizontal and vertical planes. The model was constructed using Move Petroleum Expert software and was calibrated using stratigraphic markers from three exploratory wells.

The 3D geological model was validated through the comparison between the modelled surfaces and the stratigraphic markers derived from the seismic and well data used during the model construction phase. In addition, an internal consistency analysis was carried out to verify the absence of stratigraphic inversions and the correct representation of the faults[19]. Stratigraphic and fault surfaces were generated by interpolating horizons belonging to the same lithostratigraphic units. To improve continuity of the surfaces and resolution, a structured grid of 51 intersecting geological sections (1.5 km spacing, NW–SE and NE–SW oriented) was constructed, mutually calibrated using a central reference section and refined to reduce artefacts caused by uneven data coverage. The refined surfaces were then used to generate three-dimensional volumes.

Fault geometry reconstruction

The accurate geometric representation of fault surfaces is essential for understanding tectonic evolution and for performing reliable structural analyses, especially in geologically complex settings. In this context, 3D geometric modeling of faults not only enables a better understanding of deformation mechanisms but is also fundamental for numerical simulations, structural balancing, and seismic hazard assessments[87]. The strategies used to draw surfaces vary depending on the type of geological surface being created and the structural complexity involved. In some cases, surfaces can be considered cylindrical and may be generated from a polyline and an expansion vector[88]. The use of Delaunay triangulation, although effective for initial surface generation, often results in suboptimal mesh quality due to the uneven distribution of input data, a common issue in geological datasets collected under heterogeneous conditions. To improve mesh quality and the subsequent geometric continuity between surfaces, smoothing and resampling algorithms were applied to obtain a more homogeneous discretization suitable for advanced modeling. This approach was used to reconstruct fault surfaces in the onshore area, particularly for the Meso-Cenozoic normal fault system of Mt. Kronio.

In the offshore sector, 2D interpretation of seismic lines required a spatial interpolation process to coherently connect fault segments. Here too, fault surfaces were generated using the Delaunay triangulation method. All surfaces were then resampled using a cell resolution of 200 m.

For the physical onshore-offshore correlation of corresponding fault segments, the "Ordinary Kriging" triangulation method was adopted. In this regard, the use of this method allowed for a continuous and quantitatively controlled estimation of fault geometry, enhancing the value of available spatial data and providing a reliable basis for large-scale structural analyses.

Fault analysis

We mapped 20 fault segments in the three-dimensional study area, each of which was subjected to fault analysis.

The analysis of the Leakage Factor (LF) and Slip Tendency (ST) was performed to model the propensity of faults to reactivate and transmit fluids, using the Stress Analysis module in Move software (Midland[86]). The previously constructed 3D fault surface models were analyzed to assess, respectively, their likelihood of slip (ST) and fluid migration potential (LF).

Slip Tendency was calculated as the ratio of shear stress (τ) to effective normal stress ($\sigma n'$), following the formulation of Morris et al.[89], and reflects the likelihood that a fault will slip under the present stress conditions:

$$ST = \tau/\sigma n'$$

Similarly, the Leakage Factor was determined according to the methodology proposed by Mattos et al.[77], and is defined as the ratio between fluid pressure (Pf) and the difference between effective normal stress and the tensile strength of the fault zone ($\sigma n' - T$), based on the formulations of Midland Valley[86] and Zoback[90]:

$$LF = Pf/(\sigma n' - T)$$

The stress parameters used in the calculations were obtained from the World Stress Map[91,92]. Specifically, values of $\sigma n' = 60$ N/m^2 and $\tau = 5$ N/m^2 were considered (data from https://www.world-stress-map.org/), while fluid pressure (Pf) was derived from well-log data at Orione well.

The results were normalized ($\tau/\tau max$ and LF/LFmax) to allow a color scaled 3D visualization of the fault surfaces, highlighting zones most susceptible to slip and fluid leakage.

Results

Field data

Integrated investigation of field and geophysical data suggest the Mt. Kronio tectonic unit forms a ramp-related anticline whose axial plane dips toward the northwest (Figs. 3b and 4a,b).

This unit exhibits an internal structure that allows it to be subdivided into two distinct elements: a northern sector, corresponding to the prominent relief of Mt. Kronio, and a southern sector, which lacks significant morphological expression but crops out near Contrada Mendolito and to the west of the Carabollace river (Fig. 4a,b,g).

The front of the northernmost tectonic unit is recognizable along the southern scarp that borders the Mt. Kronio relief. It trends NE–SW (Fig. 4c,h), dips to the northwest, and juxtaposes the light grey to white limestones of the Early Jurassic unit against the calcilutites and marly limestones of the Eocene deposit. The latter are only partially exposed, as they are overlain by marine terrace deposits (Fig. 4g).

Moving northeastward along the thrust fault trace, white marly limestones of the Lower Pliocene unit are observed beneath the main thrust plane. The southern portion of the unit, located downslope from Mt. Kronio, is bounded by a thrust fault synthetic to the first, which branches into several "splay faults" trending NE–SW and ENE–WSW (Figs. 3 and 4h). This geometry defines a second-order reverse fault system.

These splay faults juxtapose the calcarenites and calcirudites of the Cretaceous-Eocene unit against the deformed Plio-Pleistocene deposits, that in turn have been deformed (Figs. 3b and 4).

Compressional tectonic deformations have been recognizable since the Oligocene and define the main tectonic phase in the area. In the Mt. Kronio region, two distinct deformational events related to this contractional phase can be identified: an earlier one, characterized by uplift and the formation of unconformity surfaces, and a later one responsible for the current structural configuration of Mt. Kronio.

The earliest unconformity, obserbved in the eastern sector of Mt. Kronio, juxtaposes Jurassic limestones of Inici formation with upper Oligocene deposits in contact with Jurassic limestones. An outer more recent unconformity surface, of Messinian age, is marked by the unconformable overlying of Lower Pliocene pelagic deposits (Trubi formation) over an Meso-Cenozoic substrate, where Messinian evaporites are absent.

A general NE–SW alignment of the main thrust is observed (Fig. 4d,e,h), bounding the Mt. Kronio block and the southern block that crops-out in Contrada Mendolito (Fig. 4). These structures lasted or was reactivated during the Plio-Pleistocene, as evidenced by the involvement of the Gelasian clays, which crop out along the coastal area east of Sciacca.

The present-day structural setting of the Mt. Kronio tectonic unit is characterized by NE-SW and NW–SE jurassic extensional faults (Fig. 4h). These extensional faults are recognizable both west of Mt. Kronio, near Contrada Carrozza, and to the southeast along the old railway line.

Overall, the described structural setting depicted a tectonic system, which extends for approximately 20 km from the proximal areas of Mt. Kronio to the immediate offshore of Sciacca, allows the reconstruction of a structural setting culminating in the double-verging structural high of Mt. Kronio tectonic unit, whose prevailing kinematics are dominated by left-lateral transpression (Fig. 4f). The activity of this structure suggests that the system developed during the most recent deformational phase in the area. Its orientation, together with instrumental seismicity[93,94] and satellite geodesy data[95,96], confirms that the system is compatible with the present-day stress field.

Seismo-stratigraphyc analysis

Seismo-stratigraphic analysis of multichannel reflection seismic data led to the identification of six seismic facies units, labeled from A to F (from oldest to youngest) (Fig. 5), each defined by distinct discontinuity surfaces and seismic patterns. The units were calibrated using reinterpreted well data from the ViDEPI project (Orion and Venere wells were used to calibrate the structural high and the foredeep sector respectively), with depth-to-time conversion based on interval velocities available in the literature. This integrated approach allowed for a detailed reconstruction of the stratigraphic framework in the offshore sector.

- Unit A is characterized by high-amplitude, low-frequency reflectors with limited lateral continuity. Its thickness exceeds 1 s/TWT. Based on correlation with the Orione borehole, this unit is interpreted as corresponding to the Upper Triassic unit (Sciacca Formation).
- Unit B shows very high-amplitude, low-frequency reflectors at the top, with good lateral continuity and a thickness of approximately 1 s/TWT. It has been correlated with the Orione and Venere boreholes and is associated with the Lower Jurassic unit.

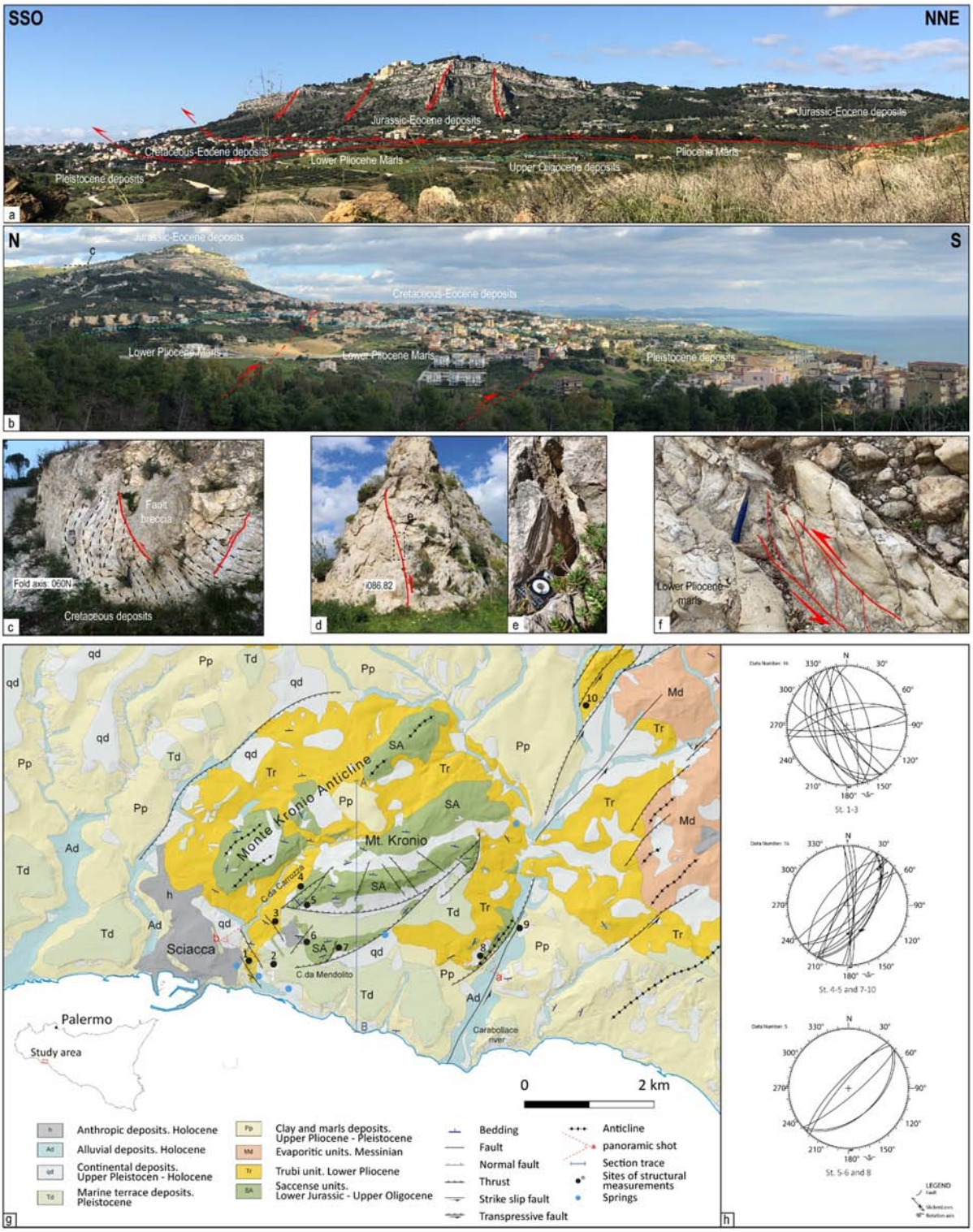

Fig. 4. Panoramic view of the southern (**a**) and western (**b**) slope of Mt. Kronio. where a Meso-Cenozoic structures was recognized. (**c**) Geometry of folds and faults affecting the marly calcilutites of Cretaceous unit; (**d**) Transpressive fault along the western limb of Mt. Kronio; (**e**) Detail of a fault plane showing kinematic indicators such as slickensides and striations; (**f**) Kinematic indicators and sinistral transpressive structures observed in the lithotypes exposed along the Carabollace River. (**g**) geological map of Mt. Kronio area displaying the sites of the mesostructural measurements and related stereoplots (**h**), and the site from where the panoramic picture shown in (**a**) and (**b**) has been shot. Map realized with Inkscape Software version 1.4 (https://inkscape.org/release/inkscape-1.4.2/windows/64-bit/msi/dl/). Dem used in the geological map is from TINITALY (https://tinitaly.pi.ingv.it/).

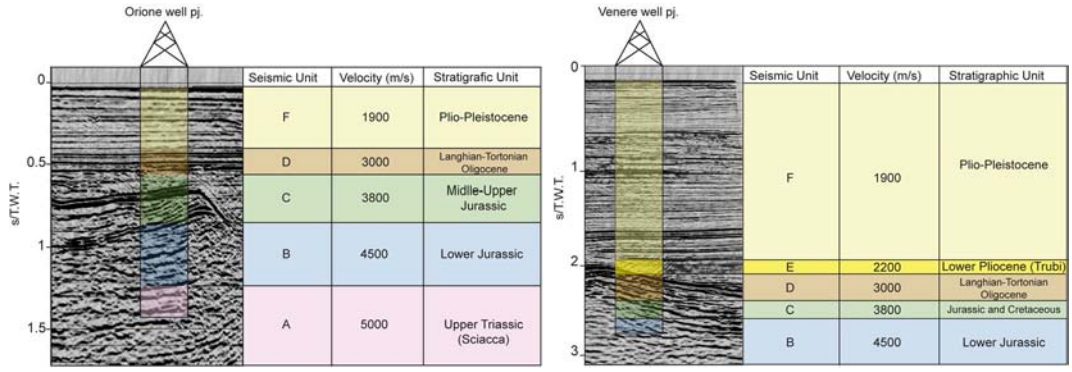

Fig. 5. Stratigraphic succession of the Orione well-log (**a**) and Venere well-log (**b**) used to calibrate seismic facies units A-F in the seismic profiles. Next to the units are shown the seismic velocities values used for conversion from m to s (TWT) of the main stratigraphic levels. Images realized with Inkscape Software version 1.4 (https://inkscape.org/release/inkscape-1.4.2/windows/64-bit/msi/dl/).

- Unit C is composed of medium-amplitude, high-frequency reflectors with poor lateral continuity and, in some cases, a transparent seismic facies. Its maximum thickness is around 0.5 s/TWT. This unit is attributed to the Buccheri Formation and, at places, also to the overlying Cretaceous-Eocene unit.
- Unit D presents high-amplitude reflectors, moderate frequency, and good lateral continuity, with an average thickness ranging between 0.2 and 0.3 s/TWT. The top of this unit is marked by an unconformity surface which displays a regional occurrence. It is interpreted as corresponding to the Upper Oligocene limestone and the Langhian-Tortonian marls unit.
- Unit E is defined by weak-amplitude reflectors onlapping the top of Unit D with limited lateral continuity and a thickness of about 0.1 s/TWT. Based on correlation with the Venere borehole, it is interpreted as corresponding to the Lower Pliocene unit (Trubi formation).
- Unit F is the thickest unit identified in the study area, with thicknesses up to 2 s/TWT. It is characterized by low-amplitude, high-frequency reflectors with good lateral continuity. Correlation with the Orione and Venere boreholes suggests that this unit includes deposits from the Plio-Pleistocene unit.

Seismo-stratigraphic interpretation of high-resolution seismic profiles in the offshore Sciacca area revealed the presence of two Plio-Quaternary seismic units, labelled from the oldest to the youngest as PQ1 to PQ2, and two additional unit M1 and M2. These units are bounded by prominent erosional unconformities and were interpreted based on seismic facies geometry, amplitude, frequency, and lateral continuity.

- **Unit PQ1** is composed of subparallel reflectors with medium frequency, variable amplitude, and good lateral continuity. The reflectors are truncated at the top by a pronounced erosional surface, marking a significant sequence boundary.
- **Unit PQ2** consists of alternating continuous reflectors of medium to high frequency and variable amplitude. Diverging reflectors within this unit suggest thickening seaward. Terminations against the overlying unit indicate another clear erosional surface.
- **Unit M1** consists of chaotic facies associated with conic external geometry.
- **Unit M2** consists of disrupted and semi-transparent to chaotic reflectors.

These units are crosscut and bounded by regionally traceable unconformities, including a major surface interpreted as the Last Glacial Maximum (LGM) erosional boundary (Fig. 7).

High-penetration seismic lines

Seismic data acquired along profiles C-529 and CSM-1 (Fig. 6) provide a comprehensive view of the structural architecture of the Sciacca offshore, revealing the presence of distinct tectonic domains and their mutual relationships. One of the most prominent structures imaged is the "Alto di Sciacca," a positive tectonic feature bounded by a set of faults. In the western sector of profile C-529, displaced reflectors associated with the Lower Jurassic unit are observed, with deformation extending upward to involve the overlying sedimentary succession up to the top of the Miocene. The structure "Alto di Sciacca" is defined by several faults that bound the uplifted block to the southeast and northwest, while in the central sector the faults exhibit a sub-vertical geometry. The measured offset across these structures reaches up to 0.3 s two-way travel time (TWT), corresponding to approximately 500 m assuming an average seismic velocity of 3800 m/s.

The structure extends for about 9 km within the study area. Its left-lateral transpressive kinematics is supported by both seismic evidence and onshore field data, where structural continuity with the offshore domain suggests a shared tectonic framework.

East of the Alto di Sciacca, a compressive structure forming a pop-up geometry is identified, involving deposits from the Lower Jurassic to the Pliocene. This structure is intersected by the Venere well (Fig. 5b), whose stratigraphic log enabled correlation with seismic reflectors and allowed the identification of key stratigraphic boundaries across the profile.

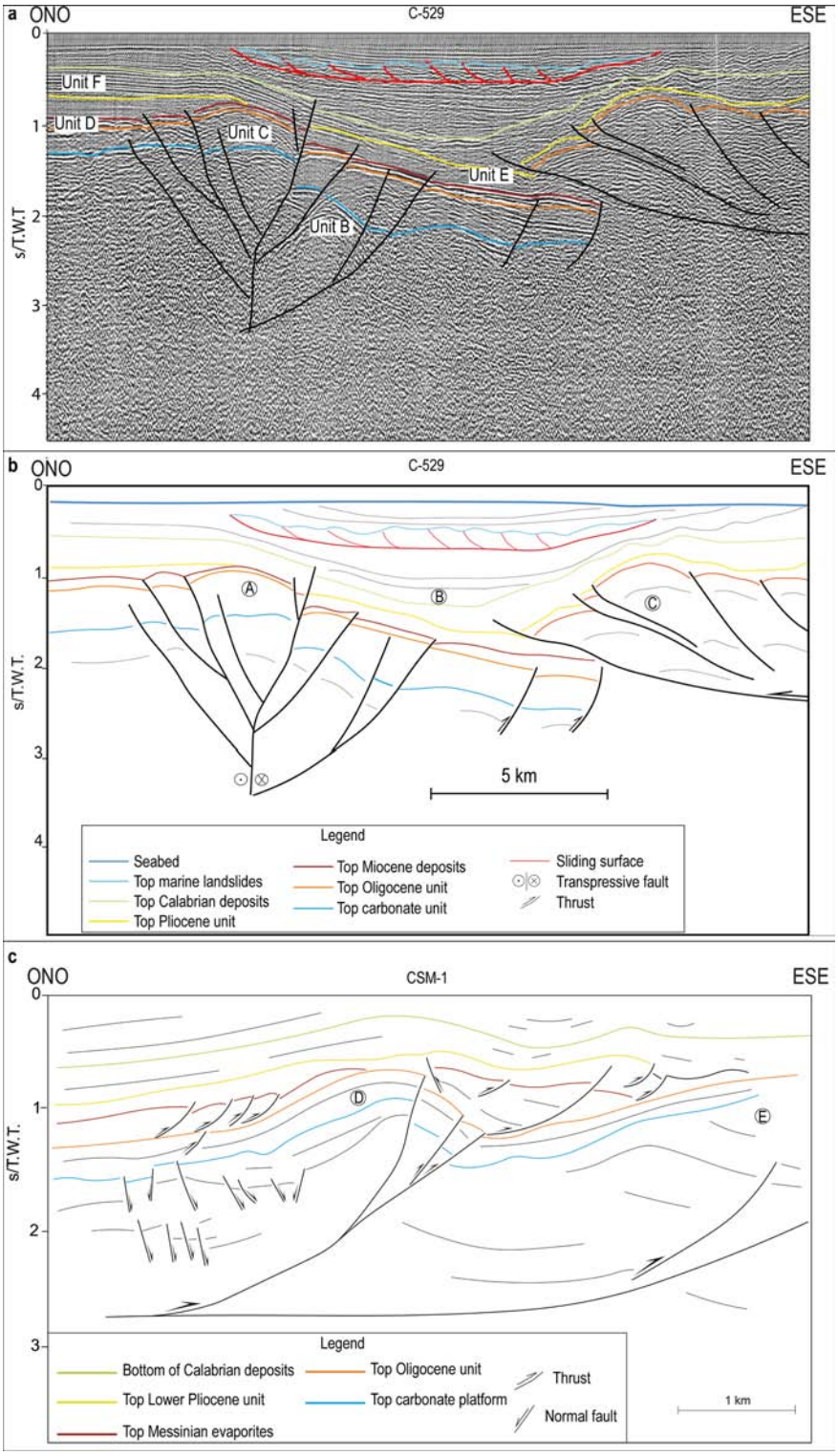

Fig. 6. Geo-seismic line drawingsof the of the C-529 (**a**,**b**) and Capo San Marco (CSM-1) (**c**) seismic reflection profile in time (TWT) (location in Fig. 2) showing the deep structural framework of the offshore and onshore study area. The labels whitin the cross section refer to: A = Alto di Sciacca; B = Gela Foredeep; C = Gela Nappe; D = Capo San Marco unit; E = Mt. Kronio unit. Images realized with Inkscape Software version 1.4 (https://inkscape.org/release/inkscape-1.4.2/windows/64-bit/msi/dl/).

Further to the east, profile C-529 also reveals the presence of an accretionary prism corresponding to the Gela Nappe, characterized by thrust-imbricated packets of strata organized in a duplex geometry. This structure affects both Miocene and Plio-Pleistocene deposits, with the most recent tectonic event within this system dated to approximately 0.8 Ma[58]. Between the front of the Gela Nappe and the Alto di Sciacca, a foredeep basin is recognized, representing the westernmost sector of the Gela Foredeep.

The continuity of compressional structures toward the inland is evidenced in profile CSM-1, which shows the tectonic structure of Capo San Marco and, partially, that of the Mt. Kronio unit, with the first tectonically overthrusting the second, both of which are detached along a basal detachment surface located at approximately 3 s/TWT. Within the Lower Jurassic carbonate sequence, several extensional basins bounded by normal faults are detected. In the central portion of the profile, a thrust sequence affects the Tortonian and Messinian deposits, displaying a divergent geometry indicative of foreland-verging propagation of compressive structures.

The reflectors corresponding to the top of the Trubi Formation, at the base of the Calabrian, as well as those immediately above, appear deformed by compressional structures involving both tectonic units. The youngest deformed sediments are dated to the Upper Calabrian (Sicilian), suggesting the compressive structures acted also during the Quaternary period. The southeast-ward prolongation of the Mt. Kronio structure is disrupted by a backthrust that offsets its structural trend, breaking the geometric continuity in that direction. Integration of field observations with seismic interpretation of the top of the Lower Jurassic limestones highlights a vertical displacement of approximately 300 m.

High resolution seismic lines (sparker)

In the central part of the western offshore sector, the most prominent morphological feature is a submerged structural high that trends NNE–SSW from the Capo San Marco coastline, where several shoals rise to depths of just -10 m. This feature is interpreted as a tectonically uplifted structure associated with NE–SW trending faults. It consists of exposed carbonate bedrock, locally covered by Posidonia oceanica meadows and, at greater depths (down to -42 m), by platform coralligenous buildups[19].

Seismic sections image the sedimentary succession beneath the seafloor down to about 100 ms TWT, corresponding to approximately 60–70 m depth, assuming an average acoustic velocity of 1700–1900 m/s through the Plio-Quaternary sediments.

This seismic line S9 (Fig. 7) is approximately 5.4 km long and displays a NW–SE orientation, located about 1.5 km offshore from Capo San Marco (Fig. 2). The underlying unit PQ1 is characterized by sub-parallel reflectors generally dipping toward the southeast. In the northwestern portion of the profile, this unit is gently folded into a broad anticline, forming a structural high. The reflectors of the lower unit are truncated at their top by a prominent erosional unconformity beneath the overlying sequence (Fig. 7).

The overlying unit PQ2 is well imaged in the eastern sector of the profile and exhibits a divergent reflector pattern, with a consistent south eastward dip. In the western portion, the line shows a wedge-shaped geometry with undulating reflectors and is bounded by angular unconformities with adjacent units.

Along the entire seismic section, fluid escape features are imaged in the water column as hydroacoustic seepage. Their presence indicates pervasive fluid circulation within the near-surface sedimentary succession. Two distinct types of mounds can be identified on the seafloor. One, located in the central portion of the profile,

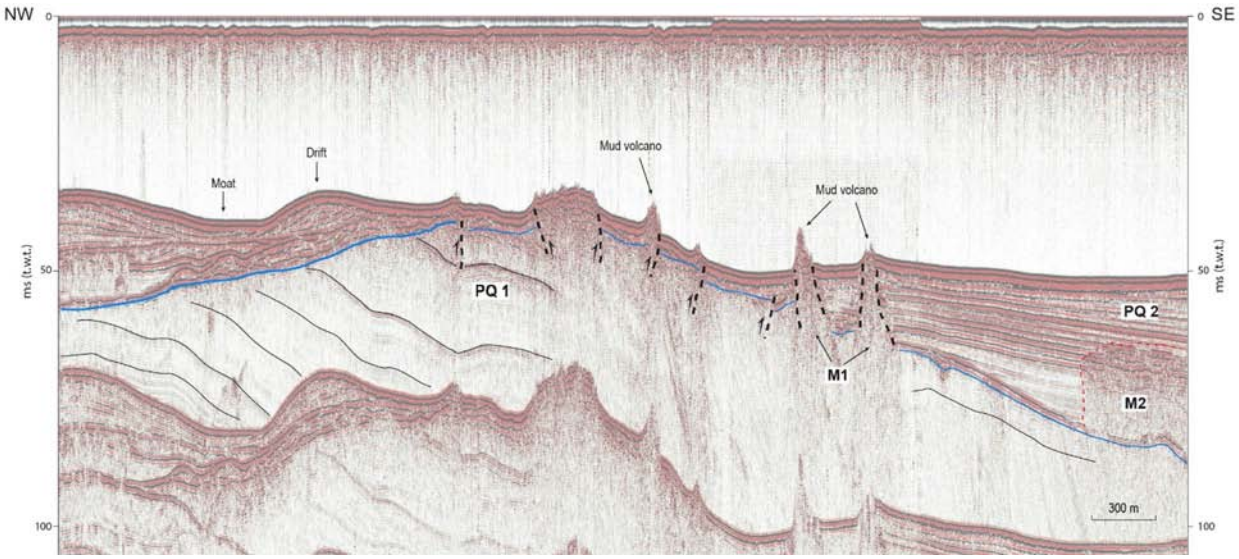

Fig. 7. Seismic interpretation of the portion of S9 high-resolution seismic profiles (location in Fig. 2). The blue line marks an erosional truncation surface separating units PQ1 and PQ2 (LGM). Solid black lines indicate the main reflectors within unit PQ1, while dashed black lines represent tectonic lineaments. In the northwestern portion, lenticular-shaped seabed deposits are identified, interpreted as contourite deposits formed by bottom current activity (moat and drift morphology).

has an almost flat top and is approximately 280 m wide. The remaining mounds exhibit conical to biconical morphologies and are associated with seismic facies indicative of active fluid expulsion (M1). These features rest on both units PQ1 and PQ2 and generate zones of acoustic blanking. These blanking zones may be related to the presence of underlying faults facilitating vertical fluid migration.

3D model

The subsurface data interpretation allowed us to build a 3D geological model in the time domain, which was depth-converted using the velocity model shown in Fig. 5. The model includes 20 faults (Fig. 8), of which 11 are compressive, with an average NNE-SSW orientation and an average length ranging between 15 and 25 km, while 9 are normal faults with main orientations of NE–SW and NW–SE.

These fault segments were grouped into three fault systems, based on their spatial position and main kinematics. The SFS comprises eight fault segments located in the offshore sector of Sciacca, including the main back-thrust of Mt. Kronio, whose onshore continuation extends southeast of Capo San Marco. The Kronio Fault System (KFS) includes nine exposed and buried fault segments within the Mt. Kronio area, including the faults cropping out in the Contrada Mendolito and Contrada Carrozza (see structural map and 3D model in Figs. 8, 9, 10).

In the northwestern portion of the study area, as revealed by seismic reflection data, the Capo San Marco Fault System (CSMFS) has been identified, consisting of three fault segments (Figs. 8 and 9).

The 3D model also includes six horizons (Fig. 8) from the Upper Triassic to the Pleistocene, namely: top of the Upper Triassic dolomit unit (Sciacca Formation), top of Lower Jurassic limestone unit, top Cretaceous-Eocene calcilutites unit, top of Upper Oligocene calcarenites unit, top of the Langhian-Tortonian marls unit, top of the Lower Pliocene marls unit.

Based on the data extracted from the 3D geological model, contour map was created for the top of the carbonate succession. This map was used to represent the 3D geometry of the main geological unit recognizable at the regional scale[70] and references therein).

The Mt. Kronio—Alto di Sciacca structural high represents the dominant morphostructural feature, controlled by a system of reverse faults that deform all modelled surfaces up to the top of the Trubi Formation.

The contour map in Fig. 11 shows the top of Upper Oligocene calcarenites unit, which represents the upper boundary of a predominantly carbonate succession assigned to the Saccense Domain. This surface is affected by significant tectonic deformation and is shaped by the main active fault systems in the Mt. Kronio–Alto di Sciacca area. The geometry of surface reflects a structurally complex setting, dominated by compressional tectonics. It serves as a key stratigraphic marker for correlating onshore and offshore structures across the foreland fold-and-thrust belt.

The elevation of the surface ranges from approximately 800 m above sea level in the northeastern sector, reaching about 200 m in correspondence with Mt. Kronio, where the formation crops out. Toward the southwestern offshore domain, within the Gela Nappe system, the surface deepens to more than 3000 m below sea level. The top is segmented into multiple tectonic blocks by the Mt. Kronio-Alto di Sciacca fault system, which accommodates both vertical and horizontal displacements.

Dip direction and inclination data reveal a differentiated structural pattern across the mapped area. The northeastern block dips southwestward (280°) with an average dip angle of approximately 7.5°, whereas the central high is characterized by southeastward-dipping surfaces (average dip direction 140°) with inclinations

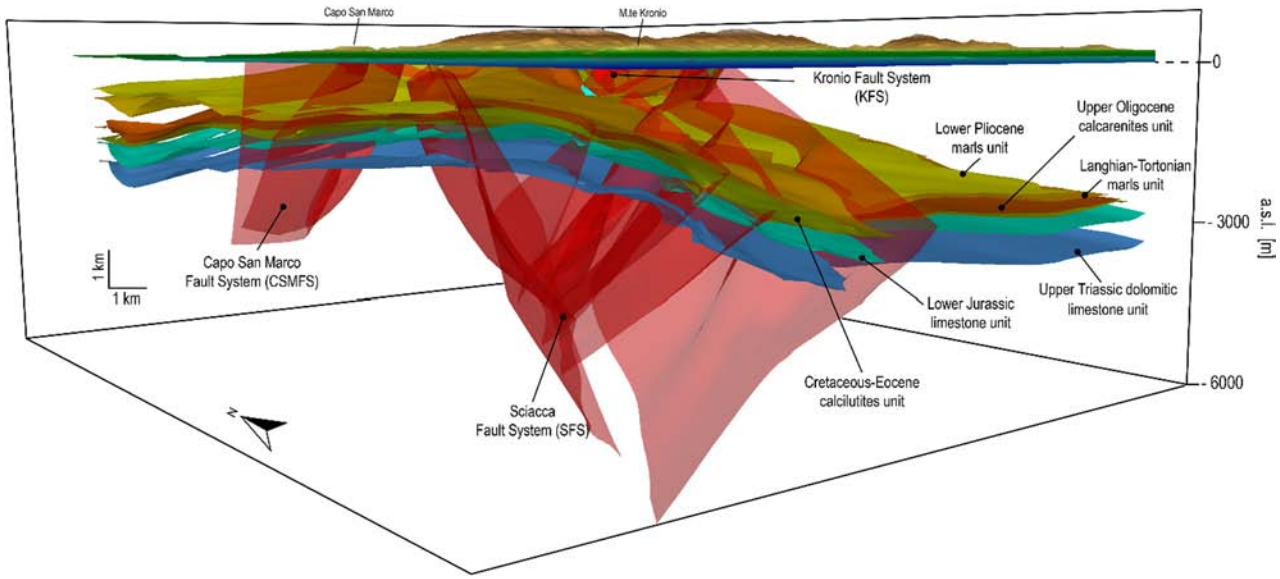

Fig. 8. View of the 3D Geological model. Image generated using Move Software version 2024.1 (https://www.petex.com/pe-geology/move-suite/move/).

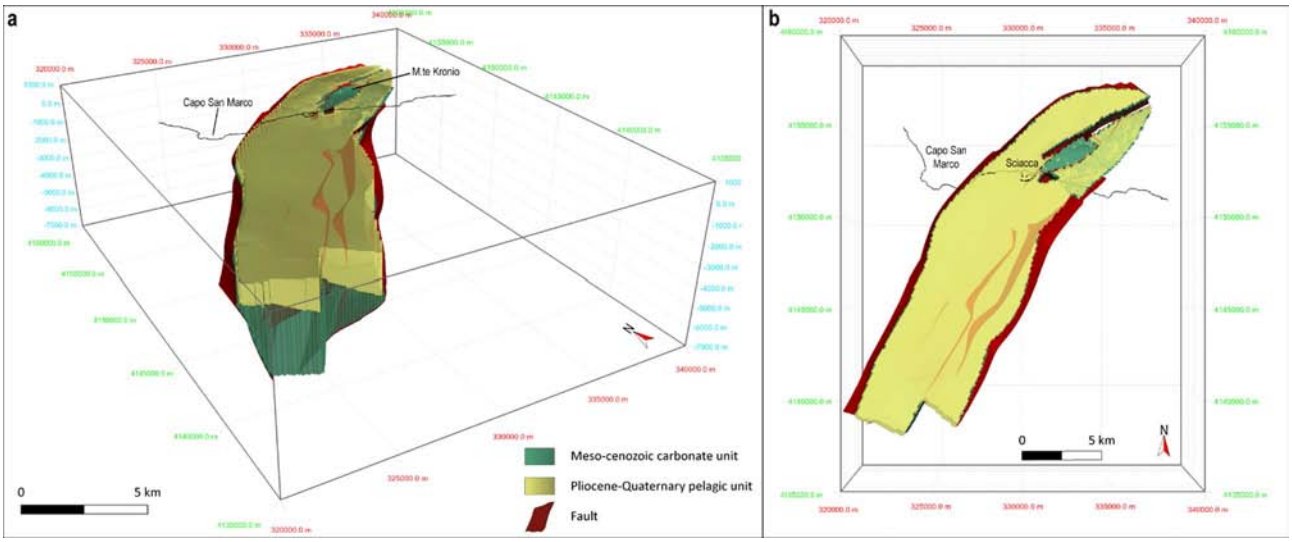

Fig. 9. Reconstructed volumes of the geothermal reservoir: views from the SW (**a**) and plan view (**b**). Image generated using Move Software version 2024.1 (https://www.petex.com/pe-geology/move-suite/move/).

ranging from 8° to 13°. These variations in dip attitude and elevation highlight the tectonic segmentation of the surface and its strong structural control by transpressive faulting.

The model shows that the top of the Langhian-Tortonian and Lower Pliocene marls unit are truncated or absent at the structural high, while they thicken laterally (Fig. 8). This pattern suggests the presence of a structural high associated with the development of an anticline structure already active during that interval, as also confirmed by field data.

Reservoir model

The modelled reservoir (Fig. 9) defines a subsurface volume with an ellipsoidal geometry, elongated along a NE–SW axis, which corresponds to the orientation of fault systems reconstructed in this sector. The body extends approximately 24 km in length and 6 km in maximum width, with an average vertical thickness of about 4 km. The areal extent of the reservoir's surface projection is roughly 95 km^2, while its total estimated volume reaches approximately 240 km^3. The modelled volume specifically corresponds to the Meso-Cenozoic carbonate succession, ranging in age from the Upper Triassic to the Upper Oligocene. This stratigraphic range includes massive platform carbonates and intensely fractured pelagic facies, known to represent effective geothermal reservoirs in the region due to their primary porosity and secondary permeability developed along fractures and karstified horizons[83]. The upper part of the modelled body is located a few hundred meters above sea level, corresponding to the outcrop of the Mt. Kronio relief, while the base reaches depths of approximately 4000 m below sea level. The geometry suggests a relatively uniform thickening along the longitudinal axis, consistent with the structural controls imposed by fault system.

Fault characterization

Statistical analysis of data structural orientation—SCAT

To investigate the orientation and distribution of fault surfaces, the Statistical Curvature Analysis Technique (SCAT) was applied to the 20 reconstructed fault planes. The analysis was conducted using dip and azimuth values extracted from the modelled geological surfaces.

The results are summarized through stereographic projections, where fault orientations are represented as poles to planes. Thrust faults exhibit a bimodal distribution of poles, indicating two dominant families striking approximately NE–SW (130°–140°) and NW–SE (310°–320°), with dip angles generally ranging between 40° and 80°. The symmetrical arrangement of pole clusters suggests the presence of conjugate thrusts with opposite vergence, consistent with a compressive regime along a NE–SW structural grain.

Normal faults show two principal orientation sets, with strike directions roughly aligned along NNE–SSW (20°–40°) and NW–SE (300°–320°). The corresponding dip angles are predominantly steep, typically between 50° and 85°, confirming the high-angle nature of these extensional structures. The spatial distribution of these poles reflects the presence of two main fault systems accommodating extensional deformation across the Mt. Kronio area.

Leakage factor

The analysis of the leakage factor, conducted on the 3D reconstructed fault surfaces using Move Software, returns a heterogeneous spatial distribution of normalized values (L/Lmax), ranging from 0 to 1. These results has highlighted the presence of potential connections between certain structural compartments, despite the presence of tectonic discontinuities that typically define their compartmentalization.

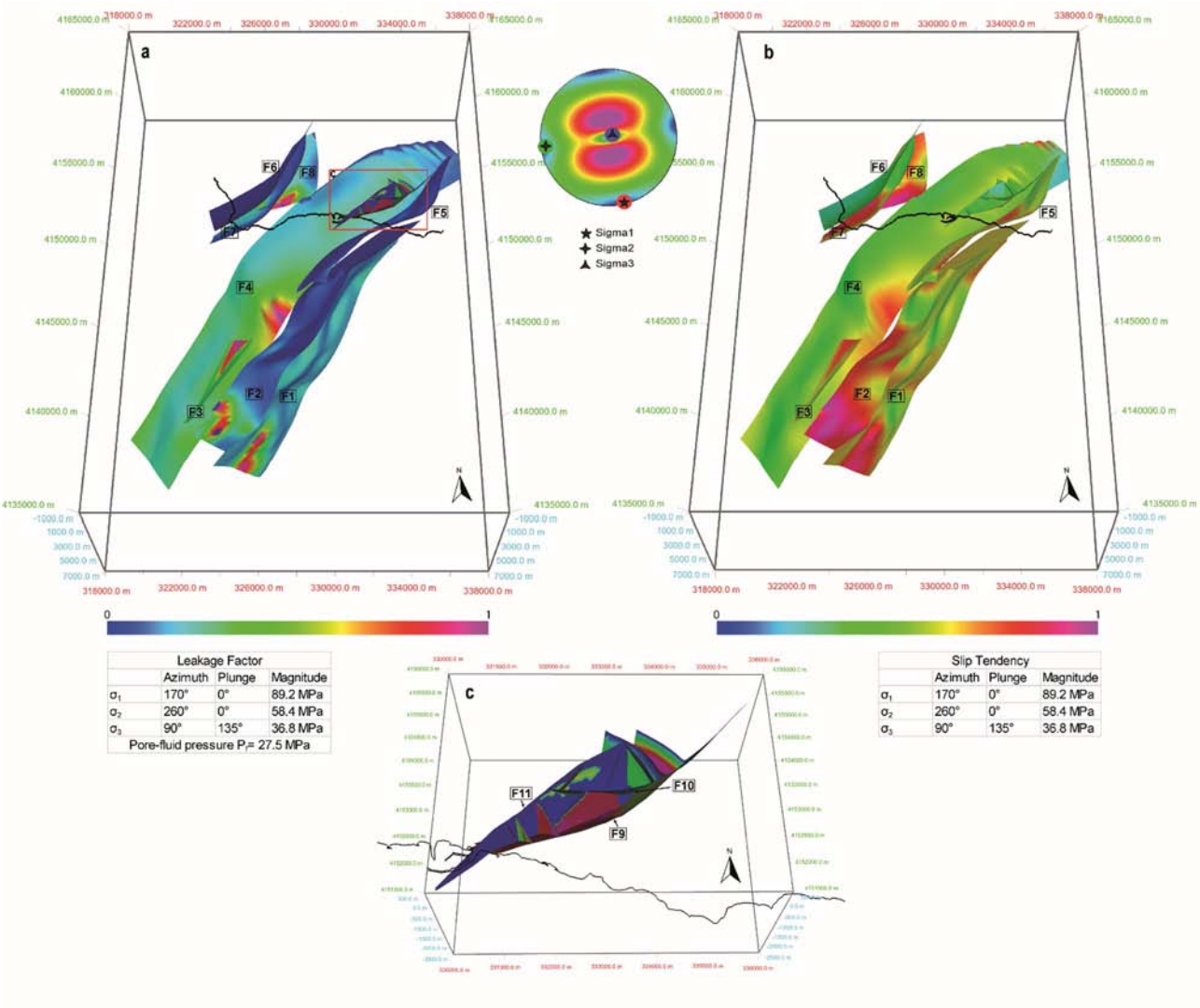

Fig. 10. (**a**) Leakage Factor model for faults in the study are considering present-day stress data from Heidbach et al., 2016. The colour scale shows normalised Leakage Factor L/Lmax. Leakage factors for the study area range from 0 to 1. (**b**) Normalised Slip Tendency (Ts/Tmax) model for the same faults, using the same stress dataset. (**c**) Zoom of the LF of the Mt. Kronio faults. Images generated using Move Software version 2024.1 (https://www.petex.com/pe-geology/move-suite/move/) and Inkscape Software version 1.4 (https://inkscape.org/release/inkscape-1.4.2/windows/64-bit/msi/dl/).

As shown in Fig. 10, lower leakage values, indicative of a low predisposition to fluid loss across the fault surfaces, are represented by cool colours (blue and cyan). These zones dominate the northeastern sector of the model, where the fault surfaces appear mechanically stable and hydraulically sealing.

In contrast, localized anomalies with higher leakage values, shown in green, yellow, and red, are concentrated in the central and southwestern parts of the fault network. Segments with leakage values exceeding 0.57 and reaching peak values near 1.00 (highlighted in magenta and fuchsia), correspond to geometrically complex zones, such as linkage areas. These areas, interpreted as zones of relatively higher permeability, act as preferential pathways for fluid migration, indicating structurally favourable sectors for the upward movement of deep fluids.

Slip tendency

Slip Tendency (TS) analysis reveals that fault surfaces with the highest potential instability (TS > 0.85) are predominantly concentrated in the southwestern and central sectors of the analyzed structure. These areas are characterized by geometric configurations that are likely favourably oriented with respect to the current stress field, indicating a higher propensity for slip under conditions of increased pore pressure or changes in the stress regime.

In contrast, the northern and eastern sectors exhibit significantly lower TS values (TS < 0.3), suggesting a reduced susceptibility to tectonic reactivation of discontinuity surfaces in these portions of the structure. This heterogeneous distribution of Slip Tendency values highlights a degree of mechanical segmentation within the

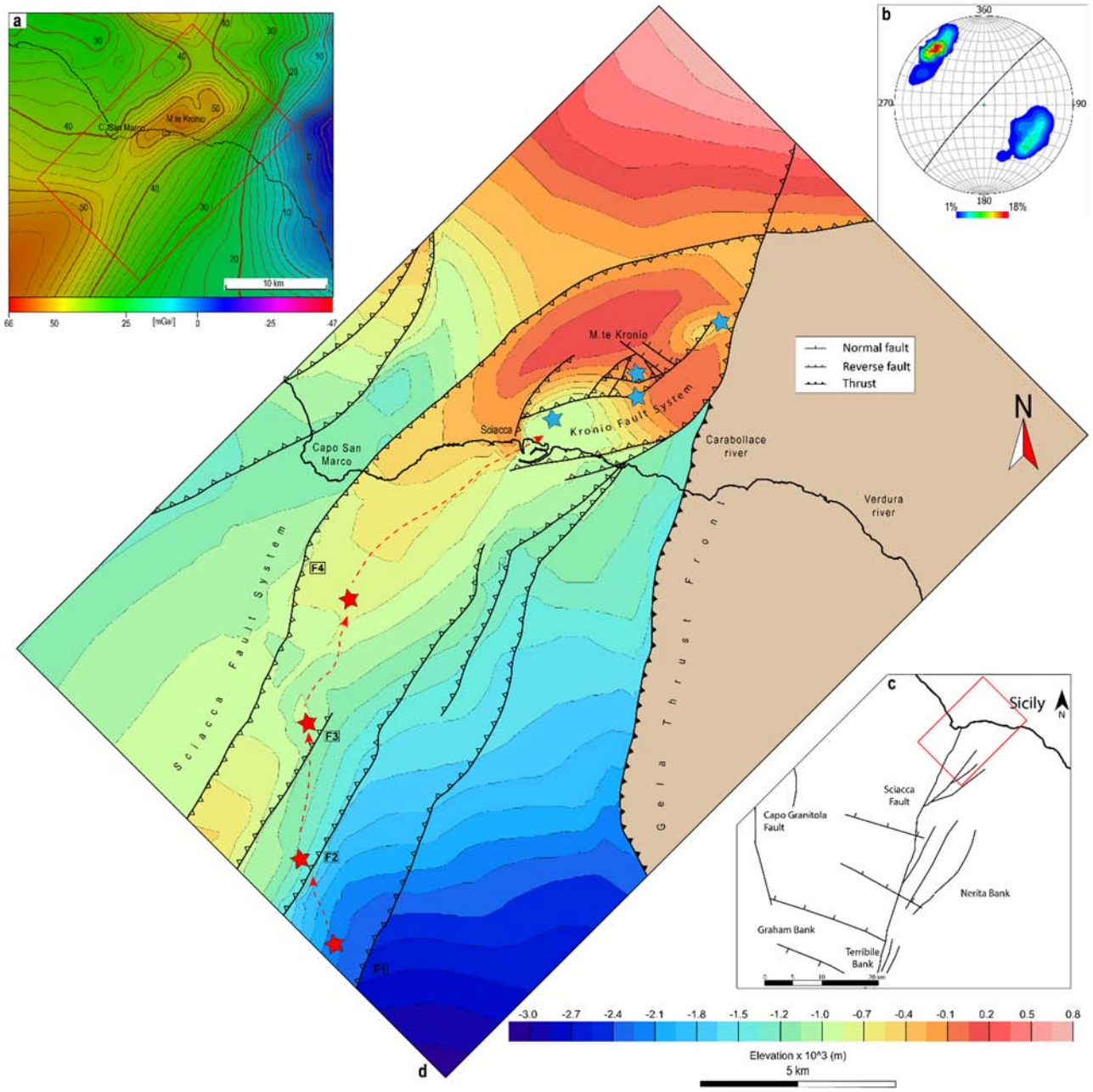

Fig. 11. Map of the top of the carbonate succession corresponding to Oligocene rocks of Irminio formation obtained from 3D model. The map shows in red stars the fault segments characterized by the highest leakage factor, and in blue stars the locations of warm fluid emissions at Mt. Kronio. The red dashed arrows indicate the inferred fluid flow path from south to north, toward the area of surface discharge. The main structural features visible in the map include the NNE–SSW alignment of the SFS and its onshore continuation beneath Mt. Kronio. (**a**) Bouguer anomaly map (from[19]) showing a prominent position anomaly along the Mt. Kronio relief and its offshore extension. Values are expressed in mGal. (**b**) Statistical analysis of the orientation of SFS in the 3D model. Equal area projection lower hemisphere. Contours represent dip direction densities for mapped Sciacca faults; black line is the mean plane. Image generated using Move Software version 2024.1. (**c**) Interpreted fault segments of the Capo Granitola and Sciacca Faults (from[50]), shown only in the offshore sector. The red rectangle corresponds to the area shown in (**d**). Maps generated using Move Software version 2024.1. and Inkscape Software version 1.4 (https://inkscape.org/release/inkscape-1.4.2/windows/64-bit/msi/dl/).

system, which may also influence its hydraulic behaviour, particularly in terms of fluid transmissivity variability along fault surfaces.

As shown in Fig. 10, the highest TS values are primarily localized in the central sector, coinciding with structural portions that also exhibit elevated Leakage Factor values. This spatial overlap between zones of higher

mechanical instability and segments of increased permeability suggests a potential correlation between a fault's reactivation propensity and its role as a conduit for fluid migration.

Fluid-related features

The analysis of high-resolution sparker seismic profiles revealed the presence of vertical seismic anomalies such as "gas chimneys" (sensu[97]) as well as horizontal acoustic anomalies and seafloor depressions associated with them. These features are commonly linked to fluid migration[98,99].

The identified acoustic anomalies exhibit two distinct seismic signal characteristics:

The first type is characterized by chaotic seismic facies with an external mound-shaped geometry. These features often display signal blanking beneath the mound, typically forming a conical or biconical shape (with two cones joined at the base). In some cases, a "Christmas Tree" facies is observed, which reflects different phases of sediment expulsion. These features match the seismic signatures associated with mud volcanoes. Formed either in continental or submerged environments, mud volcanoes result from the periodic extrusion of a mixture of liquid and gaseous hydrocarbons, water, and clay-rich mud from deeper layers onto the surface. These structures are often accompanied by anomalies in the overlying water column, interpreted as gas seepage, indications of gas escaping from the seafloor.

The second type presents a blanked seismic facies that interrupts the continuity of reflectors, with the overlying reflectors bent upward. In the upper part of the anomaly, reflectors with high-amplitude signals are often observed. These are typically linked to sudden changes in the elastic properties of the sedimentary sequence, caused by the presence of gas. Such features are interpreted as chimneys, vertical conduits for fluid migration and are frequently found near faults or other structural discontinuities.

Discussion

A new, reliable, high-resolution 3D reconstruction of the Sciacca geothermal reservoir. To establish a correlation between the NNE–SSW-trending tectonic lineaments forming the SFS in the offshore sector[50] and the investigated structure of Mt. Kronio on land, a wide dataset has been analyzed, including field observations, reflection seismic profiles, and geophysical data.

Previous studies (see Ch. 3.2) have mainly focused on the submerged segments of the SFS. Currently, focal mechanisms recorded in the offshore Sciacca area reveal a pure left-lateral strike-slip regime along NE–SW sub-vertical planes[100]. Accordingly, GPS data[95,101,102] indicate a maximum horizontal stress trending NW–SE. This pattern is consistent with an active left-lateral transpressional movement along the SFS. Moreover, the offshore portion of the SFS has been well constrained through numerical and analogue modelling approaches[50,103,104]. It has been suggested[49,50] that this fault zone, together with the Capo Granitola Fault (CGF; Fig. 8), constitutes an active lithospheric-scale shear zone extending from the Sicily Channel Rift Zone to the southern Tyrrhenian margin across western Sicily. According to some interpretations, the SFS developed along a reactivated weakness zone associated with an ancient platform-to-basin transition within the Mesozoic palaeogeographic setting of the northern African margin, recently recognized in western Sicily[59,60,83,105].

In spite of this, the real nature of the connection between the submerged and outcropping segments of this crustal tectonic feature has remained poorly constrained until now. However, field data presented in this work support the landward extension of this structure towards the Mt. Kronio area. Reflection and high-resolution seismic data indicate that the Mt. Kronio–Alto di Sciacca anticline, NE–SW oriented and deforming Upper Calabrian sediments, represents the northern, emerged portion of a 17 km-long fold known as the Sciacca Anticline North, associated with faults of the SFS[1] that continues southward toward Linosa reaching a total length of at least 200 km[49]. Gravimetric data confirm the presence of a NE–SW-trending structural high and highlight the physical continuity of Mt. Kronio with the offshore carbonate structural high of the "Alto di Sciacca". Numerous cross-cutting and abutting relationships between this system and other major tectonic elements in the area provide relative chronological constraints on deformation events, suggesting that these structures developed during the most recent active tectonic phase. Their spatial distribution, together with instrumental seismicity and geodetic data, confirms their compatibility with the present-day stress field.

The three-dimensional reconstruction of the onshore–offshore structure has allowed the definition of the main features and volumetric extent of the geothermal reservoir. The combined analysis of Leakage Factor and Slip Tendency reveals that the hydraulic behavior of the fault network is highly heterogeneous. Some faults, particularly the NW–SE master fault bounding the Mt. Kronio structure to the northwest, display consistently low leakage values, indicative of a sealing mechanical behavior. These sealing faults act as lateral barriers to fluid migration, isolating adjacent structural compartments. Within this configuration, the alternation of sealing zones and more permeable zones determines the development of confined flow pathways. The result is a structural setting comparable to a "carrier bed" system, where fluids migrate efficiently along preferential horizons and permeable fault zones, while being laterally bounded by sealing structures. This configuration provides a plausible explanation for the observed concentration of geothermal manifestations in the Mt. Kronio-Sciacca area and supports the interpretation of a hydraulically connected, but compartmentalized, geothermal reservoir extending from offshore to onshore domains.

In this context, the Mt. Kronio fault system likely connects to the surface a deeper and more complex network of discontinuities affecting the entire hydrothermal basin. Notably, the most significant thermal springs, such as the ancient Terme Selinuntine, occur in proximity to or directly along these structural lineaments. The NNW–SSE faults, attributed to this Pleistocene extensional phase, are oriented roughly orthogonal to the main NE–SW-trending thrusts and can be interpreted as secondary structures within the same regional stress regime. This structural arrangement supports the coexistence of compressive and extensional deformation styles, consistent with the tectonic evolution model proposed for the Sicily Channel Rift Zone[52].

The area shows clear evidence of fluid upwelling, as confirmed by high-resolution seismic profiles offshore Capo San Marco (see Fig. 7). The structures detected on the seafloor suggest fluid migration facilitated by faulting or fracturing within clay-rich sediments. Similar features, interpreted as mud volcanoes, have been documented in adjacent zones[25,26], indicating persistent fluid activity since the Early Pleistocene. Available evidence suggests that the offshore area is part of a wider geothermal system including the Sciacca thermal area, fed by a hot and saline aquifer hosted within Triassic carbonate rocks. This activity appears to be controlled by magmatic upwelling along active tectonic structures such as the SFS, which acts as a preferential fluid pathway[1].

Assuming the presence of a fluid source located south of the study area[1,16,50], a plausible migration model would involve a northward and upward flow direction, exploiting high-permeability fault segments. In this scenario, fluids would be progressively channeled into structural compartments laterally confined by low-permeability surfaces and overlain by pelagic units of the sedimentary cover. These geological and structural conditions would result in a partial structural trap configuration, where the forced vertical migration of fluids culminates at the surface in areas where the sedimentary cover above the carbonate substrate is absent, such as at Mt. Kronio, where surface manifestations are observed. Offshore, fluid ascent is facilitated by the combination of permeable tectonic structures and discontinuities in the impermeable cover, forming a potential preferential pathway for the escape of hydrothermal fluids, as evidenced by the numerous morpho-bathymetric features on the seafloor.

Conclusion

The stratigraphic-structural analysis of the study area of southwestern Sicily and adjacent offshore has allowed for the reconstruction of the structural setting, tectonic evolution, current kinematics, 3D model of the onshore-offshore Mt. Kronio-Alto di Sciacca structure, including the interpretation of potential flow paths for deep hydrothermal fluids ascending along tectonic lineaments.

The main conclusions of this study can be summarized as follows:

1. The integrated analysis of geological, geophysical and seismic data has, for the first time, enabled the physical reconstruction and correlation of the onshore Mt. Kronio structure with its offshore counterpart, which has been extensively documented in the literature. This correlation allowed for the delineation of a coherent three-dimensional structural framework, highlighting the continuity of the tectonic structures across the emerged and submerged sectors. Importantly, reconstructing the architecture of the geothermal reservoir in relation to the full extent of the Meso-Cenozoic carbonate body provides a volumetric and spatial basis that is fundamental for future assessments of the geothermal potential of the area. This structural coherence strengthens the interpretation of the SGF as a single geothermal domain extending across the land–sea interface, with significant implications for sustainable geothermal resource exploration and management.
2. The latest deformational event appears to involve the most recent deposits, dated to the Sicilian (Late Calabrian), in the Capo San Marco area and the most recent offshore depositional sequences. In the offshore sector, also, clear evidence of active deformation is observed on the seafloor, both immediately offshore of Capo San Marco. These data indicate that the structure is potentially and currently active.
3. The results highlight the Sciacca Fault as an active tectonic structure, with evidence of recent deformation both in onshore and offshore sectors. The integration of data has allowed for a more detailed definition of its geometry, kinematics, and relationships with surrounding structures, suggesting a key role in the current deformational framework of the Sicilian chain. The presence of active faults and potentially seismogenic segments near densely populated areas underscores the need for further investigations aimed at characterizing the expected seismicity.
4. Slip Tendency and Leakage Factor analyses suggest that the Mt. Kronio-Alto di Sciacca structure, segmented and bounded by the investigated tectonic discontinuities, may represent an effective direct pathway connecting deep fluid sources in the Sicily Channel with surface expressions in both onshore and offshore environments. Variable stress conditions acting on the faults at depth promote the migration of fluids from deeper and more southern zones toward the surface and emerged areas, leading to the formation of structural compartments capable of channeling fluids beneath the impermeable Plio-Pleistocene cover in the offshore, and allowing fluid ascent where the fractured Meso-Cenozoic substrate is exposed inland.

Overall, the recognition of active tectonic and hydrothermal structures not only refines the understanding of the current deformation pattern in southwestern Sicily but also highlights the significant geothermal potential of the Mt. Kronio- Alto di Sciacca system, which represents a promising target for future exploration and sustainable energy development.

Data availability

The datasets generated and/or analyzed during the study are available from the corresponding author, G.F.R. upon reasonable request.

Received: 24 October 2025; Accepted: 6 February 2026
Published online: 19 February 2026

References

1. Civile, D. et al. Fluid-related features in the offshore sector of the sciacca geothermal field (SW sicily): The role of the lithospheric sciacca Fault System. *Geosciences* **13**(8), 231. https://doi.org/10.3390/geosciences13080231 (2023).
2. Bigi, S. et al. Geological model of the central Periadriatic basin (Apennines, Italy). *Mar. Pet. Geol.* **42**, 107–121. https://doi.org/10.1016/j.marpetgeo.2012.07.005 (2013).

3. Calcagno, P., Bouchot, V., Thinon, I. & Bourgine, B. A new 3D fault model of the Bouillante geothermal province combining onshore and offshore structural knowledge (French West Indies). *Tectonophysics* **526**, 185–195. https://doi.org/10.1016/j.tecto.2011.08.012 (2012).
4. D'Ambrogi, C., Pantaloni, M., Borraccini, F. & De Donatis, M. 3D geological model of the sheet 280 Fossombrone (Northern Apennines)—Geological Map of Italy 1: 50,000. Atlas "Mapping geological in Italy". APAT, 193–198 (2004).
5. Galera, C., Bennis, C., Moretti, I. & Mallet, J. L. Construction of coherent 3D geological blocks. *Comp. Geosci.* **29**(8), 971–984. https://doi.org/10.1016/j.tecto.2019.05.002 (2003).
6. Wu, Q., Xu, H. & Zou, X. An effective method for 3D geological modeling with multi-source data integration. *Comput. Geosci.* **31**(1), 35–43. https://doi.org/10.1016/j.cageo.2004.09.005 (2005).
7. Zapata, S. et al. Long-term topographic growth and decay constrained by 3D thermo-kinematic modeling: Tectonic evolution of the Antioquia Altiplano, Northern Andes. *Glob. Planet. Change* **203**, 103553. https://doi.org/10.1016/j.gloplacha.2021.103553 (2021).
8. Armani, F. B., & Paltrinieri, D. Perspectives of offshore geothermal energy in Italy. In *EPJ Web of Conferences* (Vol. 54). EDP Sciences (2013).
9. Arnórsson, S. Geothermal systems in Iceland: Structure and conceptual models-I. High-temperature areas. *Geothermics* **24**(5–6), 561–602. https://doi.org/10.1016/0375-6505(95)00025-9 (1995).
10. Peacock, J. R. et al. Geophysical characterization of the Northwest Geysers geothermal field, California.. *J. Volcanol. Geotherm. Res.* **399**, 106882. https://doi.org/10.1016/j.jvolgeores.2020.106882 (2020).
11. Loreto, M. F. et al. Fault-controlled deep hydrothermal flow in a back-arc tectonic setting, SE Tyrrhenian Sea. *Sci. Rep.* **9**(1), 17724. https://doi.org/10.1038/s41598-019-53696-z (2019).
12. Takenouchi, S. et al. Identification of active faults and tectonic features through heat flow distribution in the Nankai Trough, Japan, based on high-resolution velocity-estimated bottom-simulating reflector depths. *Earth Planets Space* **75**(1), 147. https://doi.org/10.1186/s40623-023-01890-9 (2023).
13. Catalano, R. & D'argenio, B. Schema geologico della Sicilia. *Guida alla geologia della Sicilia occidentale* **24**, 9–41 (1982).
14. Catalano, R., Franchino, A., Merlini, S. & Sulli, A. Central western Sicily structural setting interpreted from seismic reflection profiles. *Mem. Soc. Geol. It.* **55**, 5–16 (2000).
15. Gasparo Morticelli, M. et al. Deep controls on foreland basin system evolution along the Sicilian fold and thrust belt. *Bull. Soc. Géol. Fr.* **186**(4–5), 273–290 (2015).
16. Bongiovanni, S. et al. Lithospheric features revealed by a new Moho map in the central-western Sicily Channel. *Sci. Rep.* **15**, 17177. https://doi.org/10.1038/s41598-025-01189-7 (2025).
17. Catalano, R., Merlini, S. & Sulli, A. The structure of western Sicily, central Mediterranean. *Pet. Geosci.* **8**(1), 7–18. https://doi.org/10.1144/petgeo.8.1.7 (2002).
18. Catalano, R. et al. Sicily's fold–thrust belt and slab roll-back: The SI. RI. PRO. seismic crustal transect. *J. Geol. Soc.* **170**(3), 451–464. https://doi.org/10.1144/jgs2012-099 (2013).
19. Sulli, A. et al. *Note Illustrative della Carta Geologica d'Italia alla scala 1:50.000, Foglio 628 Sciacca* (ISPRA, 2024).
20. Catalano, R. Tethyan Permian-Mesozoic evolution in the Sicily Pelagian continental margin (Central Mediterranean). In *European regional conference and exhibition* (2015)
21. Antonelli, M. et al. Paleogeographic evolution and structural setting of the northern side of the Sicily Channel. *Mem. Soc. Geol. It.* **41**, 141–157 (1991).
22. Argnani, A. et al. Sedimentary dynamics on the Eastern Tyrrhenian margin, Italy. PS/87 Cruise report. *Giorn. Geol.* **3**(51), 1 (1989).
23. Catalano, R., Di Stefano, P., Sulli, A. & Vitale, F. P. Paleogeography and structure of the central Mediterranean: Sicily and its offshore area. *Tectonophysics* **260**(4), 291–323. https://doi.org/10.1016/0040-1951(95)00196-4 (1996).
24. Ferranti, L., Pepe, F., Barreca, G., Meccariello, M. & Monaco, C. Multi-temporal tectonic evolution of Capo Granitola and Sciacca foreland transcurrent faults (Sicily Channel). *Tectonophysics* **765**, 187–204. https://doi.org/10.1016/j.tecto.2019.05.002 (2019).
25. Maiorana, M. et al. Seismo-stratigraphic and morpho-bathymetric analysis revealing recent fluid-rising phenomena on the Adventure Plateau (northwestern Sicily Channel). *Mar. Geophys. Res.* **45**(3), 15. https://doi.org/10.1007/s11001-024-09549-0 (2024).
26. Maiorana, M., Sulli, A., Marelli, M. & Agate, M. Geological characterization of a potential CO2 storage play in the Gela offshore (southern Sicily) and the role of a gravitational slide. *Mar. Pet. Geol.* **170**, 107127. https://doi.org/10.1016/j.marpetgeo.2024.107127 (2024).
27. Spatola, D., Micallef, A., Sulli, A., Basilone, L. & Basilone, G. Evidence of active fluid seepage (AFS) in the southern region of the central Mediterranean Sea. *Measurement* **128**, 247–253. https://doi.org/10.1016/j.measurement.2018.06.058 (2018).
28. Capaccioni, B., Vaselli, O., Tassi, F., Santo, A. P. & Delgado-Huertas, A. Hydrogeochemistry of the thermal waters from the Sciacca Geothermal Field (Sicily, southern Italy). *J. Hydrol.* **396**, 292–301. https://doi.org/10.1016/j.jhydrol.2010.11.015 (2011).
29. Caracausi, A. et al. Active geodynamics of the central Mediterranean Sea: tensional tectonic evidences in western Sicily from mantle-derived helium. *Geophys. Res. Lett.* **32**, L04312. https://doi.org/10.1029/2004GL021608 (2005).
30. Donato, A. et al. Geochemical investigations of the geothermal systems from the Island of Sicily (southern Italy). *Geothermics* https://doi.org/10.1016/j.geothermics.2021.102120 (2021).
31. Favara, R., Grassa, F. & Inguaggiato, S. Geochemical and hydrogeological characterization of thermal springs in Western Sicily, Italy. *J. Volcanol. Geotherm. Res.* **84**(1–2), 125–141. https://doi.org/10.1016/S0377-0273(98)00035-3 (1998).
32. Cusano, P. et al. Tracking the endogenous dynamics of the Solfatara Volcano (Campi Flegrei, Italy) through the analysis of ground thermal image temperatures. *Atmosphere* **12**(8), 940. https://doi.org/10.3390/atmos12080940 (2021).
33. Della Vedova, B., Vecellio, C., Bellani, S. & Tinivella, U. Thermal modelling of the Larderello geothermal field (Tuscany, Italy). *Int. J. Earth Sci.* **97**(2), 317–332. https://doi.org/10.1007/s00531-007-0249-0 (2008).
34. Siniscalchi, A. et al. Reservoir structure and hydraulic properties of the Campi Flegrei geothermal system inferred by audiomagnetotelluric, geochemical, and seismicity study. *J. Geophys. Res. Solid Earth* **124**, 5336–5356. https://doi.org/10.1029/2018JB016514 (2019).
35. Bellon, H., & Letouzey, J. Volcanism related to plate tectonics in the western and eastern Mediterranean. In *Structural History of the Mediterranean Basins*, 165–184. Technip (1977).
36. Channell, J. E., d'Argenio, B. & Horvath, F. Adria, the African promontory, in Mesozoic Mediterranean palaeogeography. *Earth-Sci. Rev.* **15**(3), 213–292. https://doi.org/10.1016/0012-8252(79)90083-7 (1979).
37. Channel, J. E. T., Oldow, J. S., Catalano, R. & D'Argenio, B. Paleomagnetically determined rotations in the western Sicilian fold and thrust belt. *Tectonics* **9**(4), 641–660. https://doi.org/10.1029/TC009i004p00641 (1990).
38. Dercourt, J. E. A. et al. Geological evolution of the Tethys belt from the Atlantic to the Pamirs since the Lias. *Tectonophysics* **123**(1–4), 241–315. https://doi.org/10.1016/0040-1951(86)90199-X (1986).
39. Chiarabba, C., Jovane, L. & Di Stefano, R. A new view of Italian seismicity using 20 years of instrumental recordings. *Tectonophysics* **395**(3–4), 251–268. https://doi.org/10.1016/j.tecto.2004.09.013 (2005).
40. Dewey, J. F., Helman, M. L., Knott, S. D., Turco, E. & Hutton, D. H. W. Kinematics of the western Mediterranean. *Geol. Soc. Lond. Spec. Publ.* **45**(1), 265–283. https://doi.org/10.1144/GSL.SP.1989.045.01.15 (1989).
41. Doglioni, C. et al. Orogens and slabs vs. their direction of subduction. *Earth-Sci. Rev.* **45**(3–4), 167–208 (1999).

42. Faccenna, C., Becker, T. W., Lucente, F. P., Jolivet, L. & Rossetti, F. History of subduction and back arc extension in the Central Mediterranean. *Geophys. J. Int.* **145**(3), 809–820 (2001).
43. Faccenna, C., Piromallo, C., Crespo-Blanc, A., Jolivet, L. & Rossetti, F. Lateral slab deformation and the origin of the western Mediterranean arcs. *Tectonics* **23**(1), 2–21. https://doi.org/10.1029/2002TC001488 (2004).
44. Roure, F., Howell, D. G., Müller, C. & Moretti, I. Late Cenozoic subduction complex of Sicily. *J. Struct. Geol.* **12**(2), 259–266. https://doi.org/10.1016/0191-8141(90)90009-N (1990).
45. Bonardi, G., Cavazza, W., Perrone, V. & Rossi, S. Calabria-Peloritani terrane and northern Ionian Sea. In *Anatomy of an Orogen: The Apennines and Adjacent Mediterranean Basins* 287–306 (Springer Netherlands, 2001).
46. Albanese, C. & Sulli, A. Backthrusts and passive roof duplexes in fold-and-thrust belts: The case of Central-Western Sicily based on seismic reflection data. *Tectonophysics* **514**, 180–198. https://doi.org/10.1016/j.tecto.2011.11.002 (2012).
47. Avellone, G., Barchi, M. R., Catalano, R., Morticelli, M. G. & Sulli, A. Interference between shallow and deep-seated structures in the Sicilian fold and thrust belt, Italy. *J. Geol. Soc.* **167**(1), 109–126. https://doi.org/10.1144/0016-76492008-16 (2010).
48. Barreca, G. & Maesano, F. E. Restraining stepover deformation superimposed on a previous fold-and-thrust-belt: A case study from the Mt. Kumeta–Rocca Busambra ridges (western Sicily, Italy). *J. Geodyn.* **55**, 1–17 (2012).
49. Civile, D. et al. Capo granitola-sciacca fault zone (Sicilian Channel, Central Mediterranean): Structure vs magmatism. *Mar. Petrol. Geol.* **96**, 627–644. https://doi.org/10.1016/j.marpetgeo.2018.05.016 (2018).
50. Fedorik, J. et al. Structural analysis and Miocene-to-present tectonic evolution of a lithospheric-scale, transcurrent lineament: The Sciacca Fault (Sicilian Channel, Central Mediterranean Sea). *Tectonophysics* **722**, 342–355. https://doi.org/10.1016/j.tecto.2017.11.014 (2018).
51. Calò, M. & Parisi, L. Evidences of a lithospheric fault zone in the Sicily Channel continental rift (southern Italy) from instrumental seismicity data. *Geophys. J. Int.* **199**(1), 219–225. https://doi.org/10.1093/gji/ggu249 (2014).
52. Corti, G., Cuffaro, M., Doglioni, C., Innocenti, F. & Manetti, P. Coexisting geodynamic processes in the Sicily Channel. *Geol. Soc. Am.* **409**, 83–94. https://doi.org/10.1130/2006.2409(05) (2006).
53. Catalano, R. et al. Contributi Alla Conoscenza Della Struttura Della Sicilia Occidentale. I: Il Profilo Palermo-Sciacca (1978).
54. Catalano, R., Di Stefano, P., & Vitale, F.P. Geological section across westernmost Sicily thrust and fold belt. *Convegno Soc. Geol. It.* Naxos Pergusa 22–25 Aprile 1987, **34** (1987).
55. Catalano, R., Di Stefano, P. & Vitale, F. P. Structural trends and palaeogeography of the central and western Sicily belt: New insights. *Terra Nova* **7**(2), 189–199. https://doi.org/10.1111/j.1365-3121.1995.tb00688.x (1995).
56. Mascle, G. Etude geologique des Monts Sicani. *Riv. It. Paleont. Strat.* (1979)
57. Monaco, C., Mazzoli, S. & Tortorici, L. Active thrust tectonics in western Sicily (southern Italy): The 1968 Belice earthquake sequence. *Terra Nova* **8**(4), 372–381. https://doi.org/10.1111/j.1365-3121.1996.tb00570.x (1996).
58. Catalano, R., Di Stefano, P., Nigro, F., & Vitale, F.P. Sicily Mainland and its offshore: a structural comparison. In *Geological development of the Sicilian-Tunisian Platform* (eds Max, M. D. & Colantoni, P.), Unesco Report in Marine Science **58**, 19–24 (1993).
59. Di Stefano, P. et al. A regional-scale discontinuity in western Sicily revealed by a multidisciplinary approach: A new piece for understanding the geodynamic puzzle of the southern Mediterranean. *Tectonics* **34**(10), 2067–2085. https://doi.org/10.1002/2014TC003759 (2015).
60. Casero, P., & Roure, F. Neogene deformations at the Sicilian-North African plate boundary. In *Peri-Tethyan Platforms: Proceedings of the IFP/Peri-Tethys Research Conference Held in Arles*, France, March 23–25, 1993, **52**, 27 Editions Technip (1994).
61. Badino G. & Torelli L. The 'Progetto Kronio: History and problems of an extreme exploration in an intact archaeological deposit. From Cave to Dolmen. Ritual and Symbolic Aspects in the Prehistory Between Sciacca, Sicily and the Central Mediterranean, Oxford, Archaeopress, 31–42 (2014).
62. Gullì, D. The prehistory of Sciacca between old acquisitions and new research. In *From Cave to Dolmen. Ritual and Symbolic Aspects in the Prehistory between Sciacca, Sicily and the Central Mediterranean* (ed. Gullì, D.) 9–29 (2014).
63. Tinè S., Tinè V. & Traverso A. *La campagna di scavo del 1986 nell'antro Fazello del complesso "Stufe di S. Calogero" del Monte Kronio di Sciacca (AG).* In *La preistoria del basso Belice e della Sicilia meridionale nel quadro della preistoria siciliana e mediterranea* (ed Tusa, S.), 245–261 (1994).
64. Floridia, G., Cacace, M., Scheck-Wenderoth, M., Bott, J. & Viccaro, M. 3D thermal model of Sicily (Southern Italy) and perspectives for new exploration campaigns for geothermal resources. *Glob. Planet. Change* **218**, 103976. https://doi.org/10.1016/j.gloplacha.2022.103976 (2022).
65. Lodolo, E., Civile, D., Zecchin, M., Zampa, L. S. & Accaino, F. A series of volcanic edifices discovered a few kilometers off the coast of SW Sicily. *Mar. Geol.* **416**, 105999. https://doi.org/10.1016/j.margeo.2019.105999 (2019).
66. Beccaluva, L., Colantoni, P., Savelli, C. & Di Girolamo, P. Upper-Miocene submarine volcanism in the Strait of Sicily (Banco senza Nome). *Bull. Volcanol.* **44**(3), 573–581. https://doi.org/10.1007/BF02600587 (1981).
67. Lanzafame, G., Rossi, P. L., Tranne, C. A. & Lanti, E. *Carta geologica dell'isola di Linosa 1: 5000* (Springer, 1994).
68. Lodolo, E., Civile, D. & Zanolla, C. Magnetic signature of the Sicily Channel volcanism. *Mar. Geophys. Res.* **33**, 33–44. https://doi.org/10.1007/s11001-011-9144-y (2012).
69. Aureli, A. Bacino idrotermale di Sciacca (Sicilia S.O.): Caratteristiche idrogeologiche e vulnerabilità, Pitagora Editrice Bologna, 152 p. (1996).
70. Montanari, D. et al. Contour map of the top of the regional geothermal reservoir of Sicily (Italy). *J. Maps* **11**(1), 13–24. https://doi.org/10.1080/17445647.2014.935503 (2015).
71. Montanari, D. et al. Geothermal resources within carbonate reservoirs in western Sicily (Italy): A review. *Earth Sci. Rev.* **169**, 180–201. https://doi.org/10.1016/j.earscirev.2017.04.016 (2017).
72. Mallarino, G. et al. Mesozoic Carbonates of the Sciacca Geothermal Field, SW Sicily (Italy). https://doi.org/10.13140/RG.2.2.25968.37123
73. Caine, J. S., Evans, J. P. & Forster, C. B. Fault zone architecture and permeability structure. *Geology* **24**(11), 1025–1028 (1996).
74. Chester, F. M. & Logan, J. M. Implications for mechanical properties of brittle faults from observations of the Punchbowl fault zone, California. *Pure Appl. Geophys.* **124**(1), 79–106 (1986).
75. Evans, R. Fluids adsorbed in narrow pores: Phase equilibria and structure. *J. Phys. Condens. Matter* **2**(46), 8989 (1990).
76. Micarelli, L., Benedicto, A. & Wibberley, C. A. J. Structural evolution and permeability of normal fault zones in highly porous carbonate rocks. *J. Struct. Geol.* **28**(7), 1214–1227 (2006).
77. Mattos, N. H., Alves, T. M. & Omosanya, K. O. Crestal fault geometries reveal late halokinesis and collapse of the Samson Dome, Northern Norway: Implications for petroleum systems in the Barents Sea. *Tectonophysics* **690**, 76–96. https://doi.org/10.1016/j.tecto.2016.04.043 (2016).
78. Kiraly, L. Karstification and groundwater flow. In *Proceedings of the Conference on Evolution of Karst: from Prekarst to Cessation*. Postojna-Ljubljana, 155–190 (2002).
79. Morin, R. H. & Savage, W. Z. Effects of crustal stresses on fluid transport in fractured rock: Case studies from northeastern and southwestern USA. *Hydrogeol. J.* **11**(1), 100–112 (2003).
80. Dipasquale, M. Caratteristiche idrotermali del bacino di Sciacca. Ph.D. Thesis, University of Palermo (2012).
81. Billi, A., Salvini, F. & Storti, F. The damage zone-fault core transition in carbonate rocks: Implications for fault growth, structure and permeability. *J. Struct. Geol.* **25**(11), 1779–1794 (2003).

82. Billi, A. & Storti, F. Fractal distribution of particle size in carbonate cataclastic rocks from the core of a regional strike-slip fault zone. *Tectonophysics* **384**(1–4), 115–128 (2004).
83. Granath, J. W. & Casero, P. Tectonic setting of the petroleum systems of Sicily. *AAPG Henberg Ser.* **1**, 390–411 (2004).
84. Salvini, F. Daisy 3, version 5.38.16. The structural data integrated analyzer [Free Software]. Dipartimento di Scienze Geologiche, Università degli Studi di "Roma3", Rome (2020).
85. Mitchum Jr, R. M., Vail, P. R., & Thompson III, S. Seismic stratigraphy and global changes of sea level: Part 2. The depositional sequence as a basic unit for stratigraphic analysis: Section 2. Application of seismic reflection configuration to stratigraphic interpretation (1977).
86. Valley, M. Midland Valley Move Application. (2024).
87. Jessell, M. Three-dimensional geological modelling of potential-field data. *Comput. Geosci.* **27**(4), 455–465 (2001).
88. Caumon, G., Collon-Drouaillet, P. L. C. D., de Le Carlier Veslud, C., Viseur, S. & Sausse, J. Surface-based 3D modeling of geological structures. *Math. Geosci.* **41**(8), 927–945 (2009).
89. Morris, A., Ferrill, D. A. & Henderson, D. B. Slip-tendency analysis and fault reactivation. *Geology* **24**(3), 275–278. https://doi.org/10.1130/0091-7613(1996)024%3c0275:STAAFR%3e2.3.CO;2 (1996).
90. Zoback, M. D. *Reservoir Geomechanics* (Cambridge University Press, 2010).
91. Heidbach, O. et al. The World Stress Map Database Release (2008). https://doi.org/10.1594/GFZ.WSM.Rel2008
92. Heidbach, O. et al. World stress map database release 2025. *GFZ Data Services* https://doi.org/10.5880/WSM.2025.001 (2025).
93. Barreca, G. et al. Geodetic and geological evidence of active tectonics in south-western Sicily (Italy). *J. Geod.* **82**, 138–149. https://doi.org/10.1016/j.jog.2011.10.007 (2014).
94. Monaco, C. & Tortorici, L. Active faulting in the Calabrian arc and eastern Sicily. *J. Geodyn.* **29**(3–5), 407–424. https://doi.org/10.1016/S0264-3707(99)00052-6 (2000).
95. Palano, M. et al. GPS velocity and strain fields in Sicily and southern Calabria, Italy: Updated geodetic constraints on tectonic block interaction in the central Mediterranean. *J. Geophys. Res. Solid Earth* https://doi.org/10.1029/2012JB009254 (2012).
96. Serpelloni, E. et al. Strain accumulation across the Messina Straits and kinematics of Sicily and Calabria from GPS data and dislocation modeling. *Earth Planet. Sci. Lett.* **298**(3–4), 347–360. https://doi.org/10.1016/j.epsl.2010.08.005 (2010).
97. Hustoft, S., Bünz, S. & Mienert, J. Three-dimensional seismic analysis of the morphology and spatial distribution of chimneys beneath the Nyegga pockmark field, offshore mid-Norway. *Basin Res.* **22**(4), 465–480. https://doi.org/10.1111/j.1365-2117.2010.00486.x (2010).
98. Judd, A. G. & Hovland, M. The evidence of shallow gas in marine sediments. *Cont. Shelf Res.* **12**(10), 1081–1095. https://doi.org/10.1016/0278-4343(92)90070-Z (1992).
99. Judd, A. G. & Hovland, M. *Seabed Fluid Flow: The Impact on Geology, Biology and the Marine Environment* 475 (Cambridge University Press, 2007).
100. Soumaya, A., Ben Ayed, N., Delvaux, D. & Ghanmi, M. Spatial variation of present-day stress field and tectonic regime in Tunisia and surroundings from formal inversion of focal mechanisms: Geodynamic implications for central Mediterranean. *Tectonics* **34**(6), 1154–1180. https://doi.org/10.1002/2015TC003895 (2015).
101. Devoti, R., Esposito, A., Pietrantonio, G., Pisani, A. R. & Riguzzi, F. Evidence of largescale deformation patterns from GPS data in the Italian subduction boundary. *Earth Plan. Sci. Let.* **311**(3–4), 230–241. https://doi.org/10.1016/j.epsl.2011.09.034 (2011).
102. Hollenstein, C. et al. New GPS constraints on the Africa-Eurasia plate boundary zone in southern Italy. *Geophys. Res. Lett.* https://doi.org/10.1029/2003GL017554 (2003).
103. Di Bucci, D. et al. Modes of fault reactivation from analogue modeling experiments: Implications for the seismotectonics of the Southern Adriatic foreland (Italy). *Quat. Int.* **171**, 2–13. https://doi.org/10.1016/j.quaint.2007.01.005 (2007).
104. Scholz, C. H., Ando, R. & Shaw, B. E. The mechanics of first order splay faulting: The strike-slip case. *J. Struct. Geol.* **32**(1), 118–126. https://doi.org/10.1016/j.jsg.2009.10.007 (2010).
105. Di Stefano, P., Cacciatore, M. S. & Zarcone, G. A Triassic carbonate platform edge in the Sciacca zone: Implications for the accretion of the Maghrebian chain in southwestern Sicily. *Rend. Online Soc. Geol. It.* **2**, 79–82 (2008).

Author contributions

G.F.R., M.M., M.G.M., M.A. and A.S.: Conceptualization, G.F.R., M.M., M.G.M.: Methodology; M.G.M., M.A. and A.S.: Validation; G.F.R.: writing-original draft preparation; G.F.R., M.G.M., M.A., V.L.P and A.S: writing-review and editing: A.S.: supervision. All authors have read and agreed to the published version of the manuscript.

Funding

This work was carried out with the financial support of the University of Palermo (PJ_AUTF_0088539) by AS, and by CARG Project—Sheet 628 Sciacca (B72C21001150001).

Declarations

Competing interests

The authors declare no competing interests.

Additional information

Supplementary Information The online version contains supplementary material available at https://doi.org/10.1038/s41598-026-39734-7.

Correspondence and requests for materials should be addressed to G.F.R.